JGR Biogeosciences

Key Points:

- The performance of individual gross primary production (GPP) models varied to capture interannual variability of GPP across different plant functional types
- Machine learning algorithm could significantly improve the capacity of estimating GPP by combining the advantages of all individual models

Correspondence to:

Z. Tian and Y. Fu,
tzhenkun@hotmail.com;
fuyy@th.btbu.edu.cn

Author Contributions:

Conceptualization: Zhenkun Tian
Data curation: Zhenkun Tian, Yingying Fu
Formal analysis: Zhenkun Tian, Chuixiang Yi, Yingying Fu, Eric Kutter
Funding acquisition: Zhenkun Tian
Investigation: Chuixiang Yi
Methodology: Zhenkun Tian
Supervision: Chuixiang Yi
Visualization: Yingying Fu
Writing – original draft: Zhenkun Tian
Writing – review & editing: Chuixiang Yi, Eric Kutter, Nir Y. Krakauer, Wei Fang, Qin Zhang, Hui Luo

Fusion of Multiple Models for Improving Gross Primary Production Estimation With Eddy Covariance Data Based on Machine Learning

Zhenkun Tian[1] , Chuixiang Yi[2,3] , Yingying Fu[4], Eric Kutter[2], Nir Y. Krakauer[5], Wei Fang[6] , Qin Zhang[7], and Hui Luo[8]

[1]School of Applied Technology, China University of Labor Relations, Beijing, China, [2]School of Earth and Environmental Sciences, Queens College, City University of New York, Flushing, NY, USA, [3]Earth and Environmental Sciences Department, Graduate Center, City University of New York, New York, NY, USA, [4]School of Mathematics and Statistics, Beijing Technology and Business University, Beijing, China, [5]Department of Civil Engineering and NOAA-CREST, The City College of New York, New York, NY, USA, [6]Department of Biology, Dyson College of Arts and Sciences, Pace University-NYC, New York, NY, USA, [7]Institution of Water and Environment Research, Dalian University of Technology, Dalian, China, [8]State Key Laboratory of Earth Surface Processes and Resource Ecology, Beijing Normal University, Beijing, China

Abstract Terrestrial gross primary production (GPP) represents the magnitude of CO_2 uptake through vegetation photosynthesis, and is a key variable for carbon cycles between the biosphere and atmosphere. Light use efficiency (LUE) models have been widely used to estimate GPP for its physiological mechanisms and availability of data acquisition and implementation, yet each individual GPP model has exhibited large uncertainties due to input errors and model structure, and further studies of systematic validation, comparison, and fusion of those models with eddy covariance (EC) site data across diverse ecosystem types are still needed in order to further improve GPP estimation. We here compared and fused five GPP models (VPM, EC-LUE, GOL-PEM, CHJ, and C-Fix) across eight ecosystems based on FLUXNET2015 data set using the ensemble methods of Bayesian Model Averaging (BMA), Support Vector Machine (SVM), and Random Forest (RF) separately. Our results showed that for individual models, EC-LUE gave a better performance to capture interannual variability of GPP than other models, followed by VPM and GLO-PEM, while CHJ and C-Fix were more limited in their estimation performance. We found RF and SVM were superior to BMA on merging individual models at various plant functional types (PFTs) and at the scale of individual sites. On the basis of individual models, the fusion methods of BMA, SVM, and RF were examined by a five-fold cross validation for each ecosystem type, and each method successfully improved the average accuracy of estimation by 8%, 18%, and 19%, respectively.

Plain Language Summary Plants uptake carbon dioxide through photosynthetic process from atmosphere, and the amount of carbon fixed is called terrestrial gross primary production (GPP) which is a key factor in global carbon cycle. People have developed many process-based models to simulate GPP at regional or global scale, and Light use efficiency (LUE) GPP models have been widely used for they are easy to implement and the input data could be conveniently accessed. How to improve the capacity of GPP model to get more precise estimation remains a change for a long time. In this study, for the purpose of improving single model capacity, we ran five popular individual GPP models (VPM, EC-LUE, GOL-PEM, CHJ, and C-Fix) across eight plant types based on site-measured and remote sensed data, and then fuse them together using three machine learning methods: Bayesian Model Averaging (BMA), Support Vector Machine (SVM), and Random Forest (RF). We found that EC-LUE performed best to simulate GPP as an individual model. RF was the best fusion method to improve estimation of GPP, followed by SVM and BMA, with the increased average accuracy of estimation by 8%, 18%, and 19%.

1. Introduction

The net land carbon balance is determined primarily by the CO_2 uptake through vegetation photosynthesis (Gross Primary Production, GPP) and CO_2 release via autotrophic respiration, litter and soil organic matter decomposition (Crisp et al., 2022; Nemani et al., 2003). Quantification of the magnitude of terrestrial carbon uptake, and how it varies spatially and temporally at global and local scales, is of the utmost importance to improve our understanding of the carbon cycle in the context of an increased atmospheric CO_2 and changing climate

(Canadell et al., 2000; Nemani et al., 2003; Yi et al., 2010). In the past decades, numerous models including physically-based methods and empirical methods (Pei et al., 2022; Running et al., 2000; Sims et al., 2006, 2008; Wei et al., 2017; Wu, Munger, et al., 2010; Wu, Niu, & Gao, 2010; Xiao, 2004; Yuan et al., 2007) have been developed and widely used to estimate global and local GPP and their seasonal variations. However, among these models, there exists tremendous inconsistency in the magnitude and spatial/temporal distribution of GPP (Keenan et al., 2012; Raczka et al., 2013).

The light use efficiency (LUE) models, in which carbon fixation is a function of the photosynthetically active radiation absorbed by green vegetation (APAR) and the efficiency of carbon uptake using absorbed light energy, are among the most widely used models to estimate GPP for its physiological logic and convenience of data acquisition and implementation (Monteith, 1972; Running et al., 2000, 2004; Wei et al., 2017). The actual light use efficiency may be reduced below the theoretical potential value by environmental factors such as temperature or water stress (Landsberg & Waring, 1997). The LUE model takes the general form as:

$$GPP = \varepsilon_g \times fPAR \times PAR \tag{1}$$

$$\varepsilon_g = \varepsilon_0 \times f(T, W, \ldots \ldots) \tag{2}$$

where PAR is the incident photosynthetically active radiation ($MJ\,m^{-2}$) per day or month, $fPAR$ is the fraction of PAR absorbed by the vegetation canopy (APAR), ε_0 is the potential LUE ($gCm^{-2}day^{-1}MJ^{-1}$) without environment stress, $f(T, W, \ldots \ldots)$ is a scalar varying from 0 to 1 that represents the reduction of potential LUE due to environmental conditions. $\varepsilon_0 \times f(T, W, \ldots \ldots)$ denotes the actual LUE ε_g under the environmental factors such as temperature, water, and others.

Several LUE models such as vegetation photosynthesis model (VPM) (Xiao, 2004; Xiao et al., 2004, 2005), GLObal Production Efficiency Model (GLO-PEM) (Cao et al., 2004; Prince & Goward, 1995), Eddy Covariance-Light Use Efficiency (EC-LUE) (Yuan et al., 2007), and the Moderate Resolution Imaging Spectro-radiometer (MODIS) product termed as MOD17 (Running et al., 2000, 2004), have been designed and developed based on different forms of LUE in Equation 2. The models differ in the expression of environmental factors such as water content of canopy, vapor pressure deficit (VPD), and temperature, and the strategies (multiplicative or minimum method) to integrate these environmental factors. The multiple choices of data source and calculation of fPAR using different vegetation index also led to different performance of LUE models. Models such as VPM, GLO-PEM, and MODIS use the multiplicative method, while the EC-LUE model take the most limiting stress factors as a reductive method based on Liebig's law. Although the water content of atmosphere and soil are key environmental constraints in vegetation photosynthesis process and are crucial for estimating global or regional patterns of GPP, the water stress factors have been quantified differently in these models with varying performances (Yuan et al., 2014; Zhang et al., 2015). The LUE models were being applied and improved by parameter calibration and optimization by many studies for a long time since the models were proposed (Cao et al., 2004; Raczka et al., 2013; Yuan et al., 2014; Zhao et al., 2005), however, little is known about the effects of further structural improvement of the LUE models on GPP estimation. Most previous studies focused on only one of the LUE models and calibrated the input parameters based on specific plant functional types (PFTs) at flux sites (Wu, Munger, et al., 2010; Wu, Niu, & Gao, 2010; Xiao et al., 2004), as a result, the advantages from different LUE models are not fully examined.

Multi-model fusion approaches have been successfully used in the area of geoscience research such as land surface parameters estimation (Duan & Phillips, 2010; Yang et al., 2016; Yao et al., 2014), and previous studies have showed that even a linear combination of single models, for instance, a simple model averaging method (SMA) or Bayesian model averaging (BMA) method, can improve the accuracy of estimation (Chen et al., 2015; Wu et al., 2012). Wu et al. (2012) utilized the BMA method to combine eight land surface long-wave radiation algorithms and obtained the best results (Wu et al., 2012). Generally, machine learning techniques that involve a nonlinear combination of single models, such as Support Vector Machine (SVM) and Random Forest (RF), perform better than those based on linear combinations of a single model (e.g., SMA or BMA) for predicting biophysical parameters (Duan & Phillips, 2010; Yang et al., 2016). Yao et al. (2017) found that the SVM method was superior to other methods to improve global terrestrial evapotranspiration estimation by integrating three process-based algorithms (Yao et al., 2017). However, previous machine learning methods were mostly focused on simulating GPP through environmental factors instead of merging process-based models (Wei et al., 2017; Wolanin et al., 2019), hence there is

a lack of multi-model fusion studies to combine the benefits of individual LUE model with different advantages, and it is of clear value to merge them to improve GPP estimation at the site level.

In this study, we used data from two primary sources: eddy covariance observations and MODIS products (reflectance and FPAR). With data from 56 global sites, we implemented five widely used GPP models: VPM, GLO-PEM, EC-LUE, CHJ, and C-Fix. We then fused the models predicting GPP in situ using three different ensemble methods: BMA, SVM, and RF separately.

Our objectives were to:

1. evaluate the performances of the single GPP models based on in situ observed or derived data and remote sensing data from 2005 to 2010;
2. fuse the single models using BMA, SVM and RF methods based on a series of cross validations; and
3. compare the accuracy of different fusion methods so as to identify the best way to combine single GPP models.

We compared the individual and fused model results against site-derived GPP to determine the accuracy of the GPP estimate. Considering MODIS GPP product is used world-wide in many geoscience research projects, we compared the MODIS GPP product as a reference against individual and fused model predictions, rather than merging it into the fusion algorithms.

2. Data and Methods

2.1. Data

2.1.1. Eddy Covariance Data

The FLUXNET2015 data set provides ecosystem-scale data on CO_2, water, and energy exchange between the biosphere and the atmosphere, and other meteorological and biological measurements around the globe (Pastorello et al., 2020). The in situ observations and derived GPP at 56 EC flux sites (Table S2 in Supporting Information S1) during 2005–2010 were selected in this study considering that the sites should involve (a) a wide climate range, (b) continuous observation for several years, and (c) diversity of plant functional types (PFTs). All the EC sites' data were downloaded from FLUXNET 2015 website (https://fluxnet.org/data/fluxnet2015-dataset/), and these sites included Cropland (CRO, 9 sites), Deciduous Broadleaf Forest (DBF, 9 sites), Evergreen Broadleaf Forest (EBF, 3 sites), Evergreen Needleleaf Forest (ENF, 18 sites), Mixed Forest (MF, 3 sites), Grassland (GRA, 9 sites), Open Shrublands (OSH, 2 sites), and Woody Savannas (WSA, 3 sites). A standardized data processing flow was applied to ensure data quality control, gap-filling of meteorological and flux measurements, partitioning of CO_2 fluxes into respiration and photosynthesis (GPP) components, and the calculation of a correction factor for energy fluxes estimating the deviation from energy balance closure. FLUXNET2015 GPP products were used to validated the estimation of individual models and fusion models. The daily products of synchronously observed meteorological data (e.g., Vapor Pressure saturation Deficit, Air temperature, Latent heat, Sensible heat, and Shortwave radiation) were utilized in this study, and missing data were removed according to the quality control (QC) flag. For all individual models, photosynthetically active radiation (PAR) was calculated from shortwave radiation (SR) as $0.45 \times SR$ (Zhao et al., 2006). Air temperature was utilized as input parameter for temperature constraint function. EC site-measured VPD was used to calculate water stress factor for GLO-PEM. The latent and sensible heat flux products of EC sites were used to compute the effective indicator of soil or vegetation moisture conditions for EC-LUE model. Site-measured CO_2 mole fraction was taken as the inputs of C-Fix and CHJ. The eddy covariance data used in this study were listed in Table 1. The detailed input parameters of the five individual models are described in Section 2.2.

Daytime method derived GPP at daily scale was used in this study to validate simulations of individual and fused models. Daytime fluxes method uses daytime and nighttime data to parameterize a model based on a light-response curve and vapor pressure deficit for GPP, and partition CO_2 flux from net ecosystem exchange (NEE) into estimates of GPP and Ecosystem Respiration (RECO) (Lasslop et al., 2010; Pastorello et al., 2020). NEE can be described by a rectangular hyperbola model:

$$NEE = \frac{\alpha \beta R_g}{\alpha R_g + \beta} + \gamma \tag{3.1}$$

Table 1
The Input Parameters of Individual GPP Models

Inputs	Description	Units	CHJ	C-Fix	GLO-PEM	VPM	EC-LUE
PAR	Converted from Shortwave Radiation (SR) using PAR $= 0.45 \times$ SR	W m^{-2}	*	*	*	*	*
T	Air temperature	°C	*	*	*	*	*
VPD	Vapor Pressure saturationDeficit	hPa			*		
LE	Latent heat fux	W m^{-2}			*		*
H	Sensible heat fux	W m^{-2}					*
CO$_2$	CO$_2$ mole fraction	μmolCO$_2$ mol^{-1}	*	*			
Number of input parameters from EC and Satellite			11	15	11	9	9

where α is the canopy light utilization efficiency, β is the maximum CO$_2$ uptake rate at light saturation, γ is the ecosystem respiration and R_g is the global radiation (Lasslop et al., 2010). Compared to estimates based on the conventional nighttime approach, the daytime method's ability to reproduce the asymmetric diurnal cycle was improved by including the vapor pressure deficit (VPD) dependency (Lasslop et al., 2010). The contribution of VPD can be described as:

$$\beta = \begin{cases} \beta_0 \exp(-k(\text{VPD} - \text{VPD}_0)), & \text{VPD} > \text{VPD}_0 \\ \beta_0, & \text{VPD} < \text{VPD}_0 \end{cases} \qquad (3.2)$$

where k parameter is estimated for each of 4-day data window to quantify the response of the maximum carbon uptake to VPD and VPD$_0$ is set to be 10 hPa. Further details of daytime algorithm can be found in Lasslop et al. (2010).

2.1.2. MODIS Data

MODIS (Moderate Resolution Imaging Spectroradiometer) is a key instrument aboard the Terra and Aqua satellites with 36 spectral bands to improve the understanding of global dynamics and processes occurring on the land, in the oceans, and in the lower atmosphere. In this study, the MODIS 8-day surface reflectance product (MOD09A1, 500 m) was used to calculate land surface water index (LSWI) for the VPM model, and the Fraction of Photosynthetically Active Radiation (FPAR) product (MOD15A2H, 500 m) was used to drive all five individual models mentioned above as fPAR in Equation 1. The Gross Primary Productivity product (MOD17A2H, 500 m) was compared with the results of the individual and fused GPP models. All these data were downloaded from Oak Ridge National Laboratory's Distributed Active Archive Center (ORNL DAAC, https://modis.ornl.gov/). Based on the site names of each flux tower, we extracted MODIS products for the 56 flux net sites in this study using the Fixed Sites Subsets Tool provided by ORNL DAAC, and data points with poor quality or missing data were excluded using the quality control (QC) flags. The daily reflectance, FPAR and GPP values were temporally interpolated from the 8-day averages using linear interpolation.

2.2. Description of the GPP Models

The eddy covariance and MODIS input data were used in the five different models described below to determine the GPP at the 56 different global sites. This supported our first objective to individually compare the performance of popular GPP models with FLUXNET2015 daytime GPP products.

2.2.1. VPM

Our first GPP model was the vegetation photosynthesis model (VPM). Leaf and forest canopies are composed of photosynthetically active vegetation (PAV, mostly chloroplast-bearing leaves) and non-photosynthetic vegetation (NPV, mostly senescent foliage, branches and stems) in the VPM and only the PAR absorbed by PAV is used for photosynthesis (Xiao et al., 2004, 2005). The actual light use efficiency ε_g is estimated as:

$$\varepsilon_g = \varepsilon_0 \times f(T) \times f(W) \times f(P) \qquad (4)$$

where $f(T)$ is estimated at each time step, using the equation developed for the Terrestrial Ecosystem Model (TEM) (Raich et al., 1991; Xiao et al., 2004).

$$f(T) = \frac{(T - T_{\min}) \times (T - T_{\max})}{[(T - T_{\min}) \times (T - T_{\max})] - (T - T_{\mathrm{opt}})^2} \tag{5}$$

where $T_{\min}$, $T_{\max}$, and T_{opt} are minimum, maximum and optimal temperature for photosynthetic activities, respectively. The effect of water $f(W)$ on plant photosynthesis uses satellite-derived land surface water index (LSWI) related to leaf and canopy water content (Xiao et al., 2002):

$$f(W) = \frac{1 + \mathrm{LSWI}}{1 + \mathrm{LSWI}_{\max}} \tag{6}$$

where $\mathrm{LSWI}_{\max}$ is the maximum LSWI within the plant growing season for individual pixels. At canopy scale, $f(P)$, which is dependent upon the longevity of leaves (deciduous vs. evergreen), is included to account for the effect of leaf age on photosynthesis:

$$f(P) = \begin{cases} \dfrac{1 + \mathrm{LSWI}}{2} & \text{(During bud burst to leaf full expansion)} \\ 1 & \text{(After leaf full expansion)} \end{cases} \tag{7}$$

The VPM model has been applied to estimate GPP for different ecosystem and performed quite well at site and regional scale (Cui et al., 2017; Xiao et al., 2004, 2005; Zhang et al., 2016; Zhou et al., 2017). In this study, the maximum of LSWI during the vegetation growing season within the available multi-year period data was taken as $\mathrm{LSWI}_{\max}$, and for the evergreen forest the $f(P)$ equaled 1. LSWI is defined as:

$$\mathrm{LSWI} = \frac{\rho_{\mathrm{nir}} - \rho_{\mathrm{swir}}}{\rho_{\mathrm{nir}} + \rho_{\mathrm{swir}}} \tag{8}$$

where ρ_{nir} and ρ_{swir} are the reflectance of NIR (0.78–0.89 μm) and SWIR (1.58–1.75 μm) spectral bands from remote sensing image (Xiao et al., 2004).

2.2.2. EC-LUE Model

The second model in our study, the Eddy Covariance Light Use Efficiency model (EC-LUE), assumes that a universal invariant potential LUE ($\varepsilon_0 = 2.14 \, \mathrm{gCm^{-2}MJ^{-1}APAR}$) exists across all the sites and biomes, which follows Liebig's law and is only affected by the most limiting factor at any given time, and the ε_g is reduced by non-optimal temperature or water stress (Yuan et al., 2007):

$$\varepsilon_g = \varepsilon_0 \times \min(f(T), f(W)) \tag{9}$$

$$f(W) = \mathrm{EF} = \frac{\mathrm{LE}}{\mathrm{LE} + \mathrm{H}} \tag{10}$$

where $f(T)$ is the same as Equation 5, LE is EC-measured latent heat flux, and H is sensible heat flux. EF is an effective indicator of soil or vegetation moisture conditions, which could be related to the Bowen Ratio (Lewis, 1995), and has been used to represent moisture conditions of ecosystems in many studies (Kurc & Small, 2004a; Suleiman & Crago, 2004). EC-LUE model has been successfully used to estimate GPP at site, regional, and global scale as the official GPP algorithm of The Global Land Surface Satellite (GLASS) Product (Li et al., 2013; Liang et al., 2013; Yuan et al., 2010).

2.2.3. GLO-PEM

Model number three in our study, the GLObal Production Efficiency Model (GLO-PEM) proposed by Prince and Goward (1995), calculates the C3 and C4 plant photosynthesis separately. The lower air temperature $f(T)$ which is the same as Equation 5, reduces stomatal conductance caused by high atmospheric water vapor pressure deficit $f(\mathrm{VPD})$, and the effect of soil moisture $f(\mathrm{SW})$ will affect actual LUE (Cao et al., 2004; Prince & Goward, 1995):

$$\varepsilon_g = \varepsilon_0 \times f(T) \times f(\delta_q) \times f(\delta_\theta) \tag{11}$$

$$f(\delta_q) = \begin{cases} 1 - 0.05\delta_q & 0 < \delta_q \leq 15 \\ 0.25 & \delta_q > 15 \end{cases} \tag{12}$$

$$\delta_q = Qw(T) - q \tag{13}$$

$$f(\delta_\theta) = 1 - \exp(0.081(\delta_\theta - 83.03)) \tag{14}$$

where δ_q is the specific humidity deficit, $Qw(T)$ is the saturated specific humidity at the air temperature, q is the specific humidity of the air, and δ_θ is the soil moisture deficit in the top 1.0 m of soil. The GLO-PEM model has been applied to estimate GPP or NPP globally and regionally using Advanced Very High Resolution Radiometer (AVHRR) or later remote sensing data in many studies (Cao et al., 2004; Goetz et al., 2000; Wang et al., 2014). Because of the lack of soil moisture deficit data at EC flux sites, here we adopted the water stress factor of the Carnegie-Ames-Stanford approach (CASA) (Potter et al., 1993) for GLO-PEM:

$$f(W) = 0.5 + 0.5\frac{\text{EET}}{\text{PET}} \tag{15}$$

where EET is estimated evapotranspiration which comes from the EC sites' derived data, and PET is the potential evapotranspiration calculated from Priestley-Taylor method (Priestley & Taylor, 1972).

2.2.4. CHJ Model

In our study's fourth model, the Cox-Huntingford-Jones (CHJ) theoretical model (Cox et al., 2000, 2006), GPP is parametrized by:

$$\text{GPP} = \text{GPP}_{\text{max}}\left[\frac{C_a}{C_a + C_{0.5}}\right]f_T \tag{16}$$

where the constant GPP_{max} is the asymptotical value of GPP as $C_a \to \infty$ without any environmental stress, C_a is atmospheric CO_2 concentration, $C_{0.5}$ is the "half-saturation" constant (taken as 500 ppm), and f_T is the air temperature scaling factor. GPP_{max} can be regarded as the maximum plant gross primary production that could be obtained with the potential LUE (ε_0) at appropriate environmental conditions, and we used the maximum value of the EC sites' GPP in growing seasons across the whole study period as GPP_{max} in this research. CHJ model takes the CO_2 fertilization effect and temperature stress as reduction factors of the optimized GPP without environmental stresses, and could be applied to estimate GPP at larger scale. We adopted the VPM model temperature and water stress factor (Equations 5 and 6) into CHJ model to calculate the estimated GPP.

2.2.5. C-Fix Model

The fifth and final model, the Carbon-Fixation Model (C-Fix), uses the temperature dependency factor and CO_2 fertilization effect to estimate carbon flux (Veroustraete et al., 1996, 2002) and calculate GPP:

$$\varepsilon_g = \varepsilon_0 \times f(T) \times f(CO_2) \tag{17}$$

The temperature dependency factor is described as:

$$f(T) = \frac{e^{\left(C_1 - \frac{\Delta H_{a,P}}{R_g T}\right)}}{1 + e^{\left(\frac{\Delta S T - \Delta H_{d,P}}{R_g T}\right)}} \tag{18}$$

where C_1 is a constant, T is air temperature, $\Delta H_{a,P}$ and $\Delta H_{d,P}$ are activation and deactivation energy respectively, R_g is the gas constant, and ΔS is Entropy of the denaturation equilibrium of CO_2. CO_2 fertilization is defined as the increase in carbon assimilation due to CO_2 levels above the atmospheric background level or reference level:

$$f(CO_2) = \frac{[CO_2] - \frac{[O_2]}{2\tau}}{[CO_2]^{\text{ref}} - \frac{[O_2]}{2\tau}} \times \frac{K_m\left(1 + \frac{[O_2]}{K_0}\right) + [CO_2]^{\text{ref}}}{K_m\left(1 + \frac{[O_2]}{K_0}\right) + [CO_2]} \tag{19}$$

where τ is CO_2/O_2 specificity ratio, $[CO_2]$ and $[CO_2]^{\text{ref}}$ are CO_2 and referenced CO_2 concentration respectively, $[O_2]$ is O_2 concentration, K_m is the affinity constant for CO_2 of Rubisco, and K_0 is the inhibition constant for O_2. We obtained the validated parameters of the C-Fix model mentioned above from previous literature (Veroustraete et al., 2002).

2.3. Three Machine Learning Fusion Algorithms

To complete our second objective, those five GPP models were then fused and optimized using the following three machine learning fusion algorithms.

2.3.1. Bayesian Model Averaging (BMA) Method

The BMA method considers a predicted variable y, the corresponding evidentiary target data y_T, and an ensemble of K model simulations $\{f_1, f_2 \cdots f_K\}$ of variable y. The probabilistic prediction of y based on the multi-model ensemble, given target data y_T, can be expressed as (Duan & Phillips, 2010; Raftery et al., 2005):

$$p(y|f_1, f_2 \cdots f_K) = \sum_{(k)} p(y|f_k) \cdot p(f_k|y_T) \tag{20}$$

where $p(y|f_k)$ is the probabilistic prediction given by model k alone, and $p(f_k|y_T)$ is the likelihood that this simulation is the best. Taking $p(f_k|y_T)$ as a fractional statistical weight $w_k\left(\sum w_k = 1\right)$, and (18) can be written as

$$p(y|f_1, f_2 \cdots f_K) = \sum_{(k)} p(y|f_k) \cdot w_k \tag{21}$$

Thus, the prediction is a weighted sum of the predictions of y provided by the individual models, and can be calculated using the maximum likelihood function with the expectation maximization (EM) algorithm (Raftery et al., 2005). In this study, the individual model predictions act as the $\{f_1, f_2 \cdots f_K\}$, and EC-derived GPP is the target data y_T. R package MBA was used to conduct averaging over five different GPP models here to merge them.

2.3.2. Support Vector Machine (SVM)

SVM, our study's second fusion algorithm, is good at classifying multi-dimensional data as an optimal boundary classification method based on VC (Vapnik-Chervonenkis) dimension theory and structural risk minimization criteria, and can be used to resolve the original nonlinear problem in a new feature space (Suykens, 2001; Vapnik, 1994). Giving a training set of instance-label pairs (x_i, y_i), $i = 1, 2, \cdots l$ where x_i is a n-dimensional vector, $x_i \in R^n$ and $y_i \in \{-1, +1\}$, to obtain the functional dependency $f(x) = (w \cdot x) + b$, the SVM require the following optimization problem to be solved:

$$\min\left(\frac{1}{2}w^T w + C\sum_{i=1}^{l} \xi_i\right)$$

$$\text{subject to } y_i\left(w^T \phi(x) + b\right) \geq 1 - \xi_i, \quad \xi_i > 0 \tag{22}$$

where w is the weights vector, b is the bias, C is the penalty parameter of the error term, $\phi(x)$ maps the training x_i into a higher dimensional space, ξ_i is the error term. Furthermore, $K(x_i, x_j) = \phi(x_i)^T \phi(x_j)$ is called the kernel function, and we took the radial basis function (RBF) in this study for it is the most widely used kernel and performs better in previous studies (Khalil et al., 2006; Yao et al., 2017). The RBF kernel can be expressed as:

$$K(x_i, x_j) = exp\left(-\gamma \|x_i - x_j\|^2\right), \gamma > 0 \tag{23}$$

Table 2
The Maximum LUE, Minimum, Maximum and Optimal Temperature Parameters Look-Up Table for Each Plant Functional Type (PFT)

PFT	ε_0 (gC/m^2/d/MJ)	T_{min}(°C)	T_{max}(°C)	T_{opt}(°C)
CRO	1.931(C3) 2.8966(C4)	−1	48	30
DBF	1.931	−1	40	20
EBF	1.931	−2	48	28
ENF	1.931	−1	40	20
GRA	1.931(C3) 2.8966(C4)	0	48	27
MF	1.931	−1	48	19
OSH	1.931	1	48	31
WSA	1.931	−1	48	24

where γ is the kernel parameter. Further details about the SVM algorithm can be found in previous literature (Cortes & Vapnik, 1995; Vapnik, 1995). The R package e1071 offers an interface to implement the SVM algorithm, and we took individual GPP models' outputs x_i as the inputs of SVM, which would map the training x_i into a higher dimensional space automatically and generate the fused GPP.

2.3.3. Random Forest (RF)

Our study's third and final fusion method, RF, is a classifier consisting of a collection of tree-structured classifiers $\{h(x, \Theta_k), k = 1, 2 \cdots \}$ where $h(x, \Theta_k)$ is a classifier, Θ_k is the kth independent identically distributed random vector, and x is an input vector (Breiman, 2001). Random Forest is a robust machine learning algorithm that can be used for a variety of tasks including regression and classification. It is an ensemble method, and contains a large number of small decision trees representing a distinct instance of the classification of data input into the random forest. RF algorithm was proposed by Breiman in 2001 and was widely applied in the fields of geographical science research because the algorithm is extremely robust, easy to get started with, good at heterogeneous data types, and has very few hyperparameters (Amini et al., 2022; Gyamerah, 2020; Meng, 2021). R package randomForest (Liaw & Wiener, 2002) gave the interface to bring individual model GPP into the process of putting the input vector down each of the trees in the forest, and ultimately output the merged value.

2.4. Parameterization of the GPP Models

In this study, the maximum light use efficiency (ε_0) needs to be estimated for individual plant functional types. Since C4 plants have no photorespiration and less saturation effect compared to C3 plants, the differences between C3/C4 plants in utilizing solar energies should also be considered (Prince & Goward, 1995; Zhang et al., 2017). Similarly, the minimum, maximum, and optimal temperature of photosynthetic activities vary among different vegetation types. We adopted a look-up table (Table 2) to determine maximum LUE according to plant functional types and C3/C4 plants based on previous literature (Wu, Munger, et al., 2010; Wu, Niu, & Gao, 2010; Xiao et al., 2005; Yuan et al., 2007; Zhang et al., 2017). The C4 vegetation percentage map from International Satellite Land-Surface Climatology Project, Initiative II (ISLSCP II) data were used to approximately express the C3/C4 plants' area ratio for each EC flux site, and the corresponding LUE could be obtained based on the area-weighted averages (Zhang et al., 2017). Although the spatial resolution of ISLSCP II data is coarser than flux site footprints, it is the best C4 vegetation distribution map that covers the global EC flux sites at present. Thus, we made the parameters set, which are essential inputs for running individual LUE models in this study.

2.5. Statistical Analysis and Cross Validation

Our third and most important objective was to test how the individual and fused models perform compared with FLUXNET2015 GPP products. Since this study focused on the comparison and fusion of GPP models to reach better estimations instead of optimizing individual model parameters, we used a generic-parameters set for all the models across eight PTFs. As the global standard remote sensing product, MODIS GPP was taken as the reference value to be compared with other modeled and ensembled GPP.

Three statistical metrics were used to evaluate the performance of the individual GPP models and also the fusion methods in this study: the square of the correlation coefficients (R^2); root mean square error (RMSE); and relative predictive error (RPE). The RMSE and RPE are computed as:

$$\mathrm{RMSE} = \sqrt{\frac{\sum\limits_{i=1}^{n}(\hat{y}_i - y_i)^2}{n}} \tag{24}$$

$$\mathrm{RPE} = \frac{\overline{\hat{y}} - \overline{y}}{\overline{y}} \times 100\% \tag{25}$$

where $\hat{y}_i$ and y_i represent modeled GPP and derived GPP at EC sites, respectively. $\overline{\hat{y}}$ and $\overline{y}$ are average of modeled values and observed values, and n indicates the sample size. Higher R^2, lower RMSE, and lower absolute value of RPE are the indicators of better model performance.

We evaluated the performance of the three fusion algorithms using a five-fold cross validation method, in which the data set was randomly divided into five groups with equal number of samples. We independently validated GPP estimations of the fusion models by using each of the five groups after training models with the remaining four groups, computed the three metrics mentioned above, and then summarized the mean value of R^2, RMSE, and RPE for individual GPP models, BMA, SVM, and RF fusion methods. To further evaluate the performance of the fusion methods, we used the site-observed and modeled data to test two categories of GPP variability based on PFTs and EC sites, respectively.

2.6. Akaike's Information Criteria (AIC) and Bayesian Information Criteria (BIC)

To further explore the fused performance of BMA, SVM, and RF, the AIC and BIC, which are two terms that address evaluation and selection from optional models, were used here to evaluate the three fusion methods. The AIC is a way of selecting a model from a set of models based on information theory and defined as (Akaike, 1974):

$$\text{AIC} = -2\ln(L) + 2k \tag{26}$$

where L is the maximum likelihood function and k is the number of free parameters in the model. A lower AIC means the model has better capacity of prediction. The BIC is another indicator to select a model (Schwarz, 1978), but it considers the sample size n, and is defined as:

$$\text{BIC} = -2\ln(L) + k\ln(n) \tag{27}$$

The model with lower BIC should be selected, thus, the lowest AIC and BIC values indicate the best performance of different fusion methods in this study.

3. Results

3.1. Comparison of the Individual and Fusion Methods Based on PFTs

Table S1 in Supporting Information S1 and Figure 1 show the estimated accuracies of the five individual models, MODIS GPP product, and three fusion methods across eight PFTs using R^2, RMSE, and RPE compared with FLUXNET2015 daytime GPP products. For the five individual models, EC-LUE, GLO-PEM, and VPM explained most GPP variations across all vegetation types, characterized by the average R^2 of 0.68, 0.60, and 0.57, while C-Fix and CHJ explained no more than half of the variations with the average R^2 of 0.50 and 0.43. MODIS GPP R^2 was 0.59 and similar to GLO-PEM and VPM, less than EC-LUE, which showed EC-LUE, GLO-PEM, and VPM performed as well as or even better than MODIS GPP among eight ecosystem types. For the three fusion methods, all of them clearly improved the ability of explaining GPP variations with average R^2 of 0.73, 0.81, and 0.80 from BMA, RF, and SVM. As for average RMSE and RPE, EC-LUE was the best performer in individual models (2.43 gC m^{-2} day^{-1}, 0.02), followed by MODIS GPP (2.57 gC m^{-2} day^{-1}, −0.11) and VPM (2.68 gC m^{-2} day^{-1}, −0.04), and then GLO-PEM (2.60 gC m^{-2} day^{-1}, 0.09) and C-Fix (4.96 gC m^{-2} day^{-1}, 0.82). CHJ ranked last (5.72 gC m^{-2} day^{-1}, 1.19). RF reduced the RMSE to 1.60 gC m^{-2} day^{-1} and RPE to almost zero as the best performing fused model with the average R^2 of 0.81. SVM improved the estimation accuracy with similar R^2 of 0.80 but higher average RMSE and more deviated RPE. BMA also significantly improved the accuracy of GPP estimation but not as well as RF and SVM. Apart from the MODIS GPP product and VPM estimation, all of the other individual models overestimated GPP compared with site observations, while the three fusion methods narrowed the bias between estimation and observation.

Figure 2 and Figure S1 in Supporting Information S1 showed that the individual model performances greatly varied across different plant cover types. For the individual models across mixed forest (MF) in Figure 2, R^2 of EC-LUE was the highest (0.71), while R^2 of CHJ and C-Fix were the lowest (0.57 and 0.61), but MODIS held the lowest RMSE (2.28 gC m^{-2} day^{-1}), and VPM had the lowest RPE (almost 0). The statistical metrics indicated that EC-LUE, MODIS, VPM, and GLO-PEM were top performers for estimating GPP, followed by C-Fix, while CHJ exhibited the poorest accuracy of the models. CHJ greatly overestimated GPP compared with site-derived
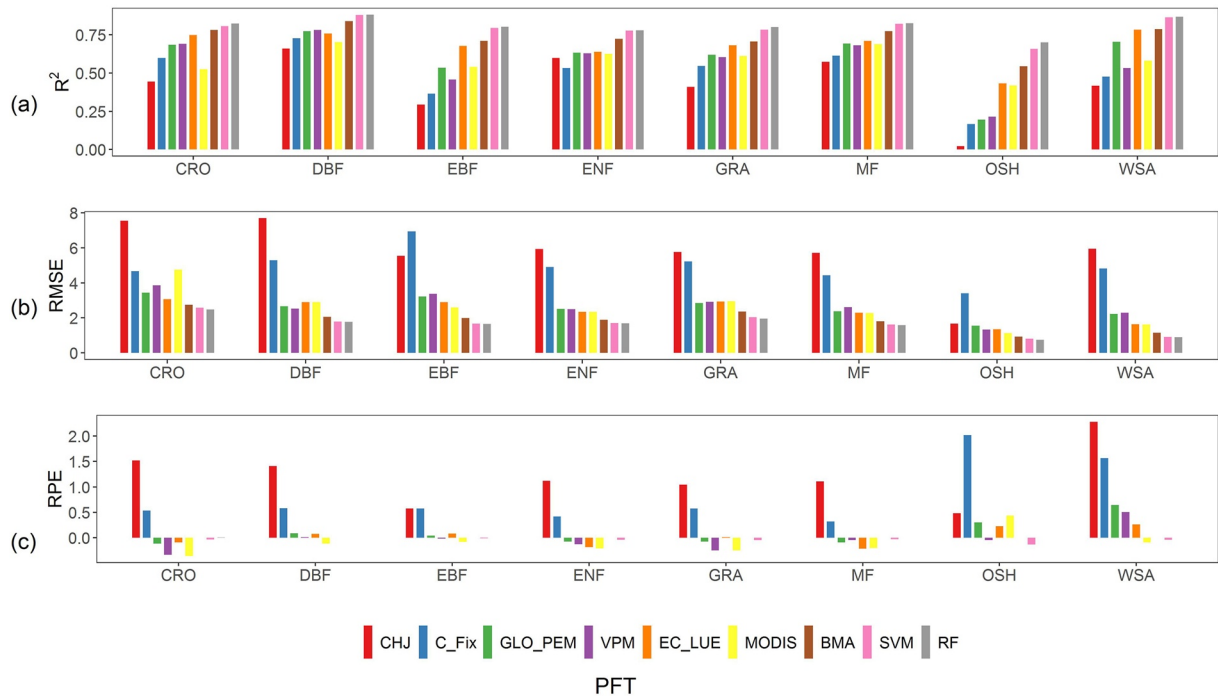
Figure 1. The square of the correlation coefficients (R^2), root mean square error (RMSE, gC m^{-2} day^{-1}), and relative predictive error (RPE) of individual models, MODIS GPP, and fusion models in estimating GPP across the eight ecosystem types.

GPP with highest RPE (1.11) and highest RMSE (5.18 gC m^{-2} day^{-1}). BMA raised the accuracy of estimation explaining 77% variance of site-derived GPP with the relative prediction error close to 0, while SVM and RF further improved the accuracy by raising R^2 to 0.82 and 0.83, and reducing RMSE to 1.62 and 1.59 gC m^{-2} day^{-1}, respectively. Meanwhile, RF decreased the RPE to almost zero.

For other forest PFTs (ENF, EBF, DBF) in Figure S1 in Supporting Information S1, considering the accuracy metrics, EC-LUE performed best on land cover type of ENF and EBF compared with other individual models, while VPM was the best one in DBF. The fusion methods of BMA, SVM, and RF clearly improved the estimation accuracy with higher R^2, and lower RMSE and RPE.

The predicted GPP of CHJ model could hardly explain the variance of observed GPP on OSH cover type, and the lowest R^2 (0.02) indicated its weak modeling capacity. EC-LUE explained nearly half of the variance in OSH (0.43), but still took higher RMSE (1.35 gC m^{-2} day^{-1}) than MODIS GPP (1.14 gC m^{-2} day^{-1}). As for Cropland (CRO), EC-LUE performed the best reflected by R^2 (0.75), RMSE (3.06 gC m^{-2} day^{-1}), and RPE (−0.09), while GLO-PEM conducted the second-best performance, followed by VPM, MODIS, and C-Fix. CHJ still ranked last. In Grassland (GRA) and Woody Savannas (WSA), the individual models ordered into three classes: EC-LUE took the first class; VPM, GLO-PEM, and MODIS were in the second rank, and C-Fix and CHJ were on the bottom. For all PFTs, BMA, SVM, and especially RF improved the GPP estimation to a great extent.

Figure 3 showed the increased R^2 percentage achieved by the fusion algorithms compared to the average and maximum values of five individual models, and decreased RMSE percentage compared to the average and minimum value of those individual models. For example, RF increased R^2 by 19% and 45% compared to maximum value of EC-LUE and average of five single models respectively. Panel (b) of Figure 3 indicated that the fusion methods also significantly reduced the RMSE compared to the minimum and mean value from individual models (RF, for instance, by 34% and 57%).

Figure 4 showed the probability of density curves of predicted GPP errors in VPM, EC-LUE, GLO-PEM, CHJ, C-Fix, MODIS, BMA, SVM, and RF algorithms compared with in situ measurements. For single models, EC-LUE, VPM, and GLO-PEM all had curve peaks centered on zero, but GLO-PEM and C-Fix had slightly thicker tails on the right side, which indicates overestimation compared to site measurements. EC-LUE and VPM had balanced biases on both sides, which means a good error distribution. MODIS GPP had lower peaks centered
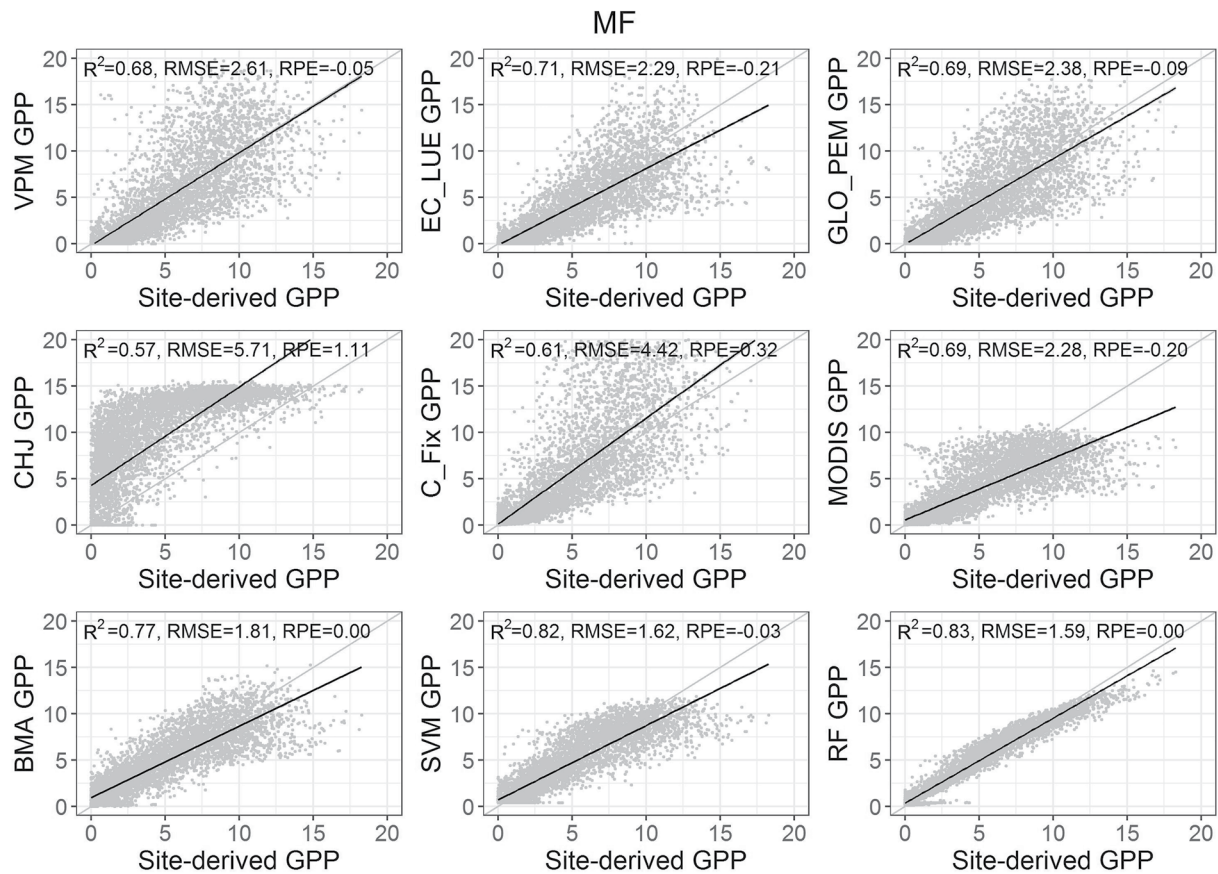
Figure 2. The scatter plots of the square of the correlation coefficients (R^2), root mean square error (RMSE, gC m^{-2} day^{-1}), and relative predictive error (RPE) across Mixed Forest (MF) cover type between daily site-derived GPP (gC m^{-2} day^{-1}) at flux sites and the estimates from five individual models, MODIS GPP product, and three fusion methods.

on zero compared with EC-LUE, and took a thick left side curve suggesting occasional underestimation. CHJ, with a prominent ascendant probability density at right side and a barely visible peak, overestimates GPP within a large range and was the poorest performing model. BMA has a wide shoulder instead of a zero-centered peak, which made it the worst one among three fusion methods. The error distributions of the SVM- and RF-fused GPP estimation were more closely centered on zero and especially the RF method decreased the substantial positive
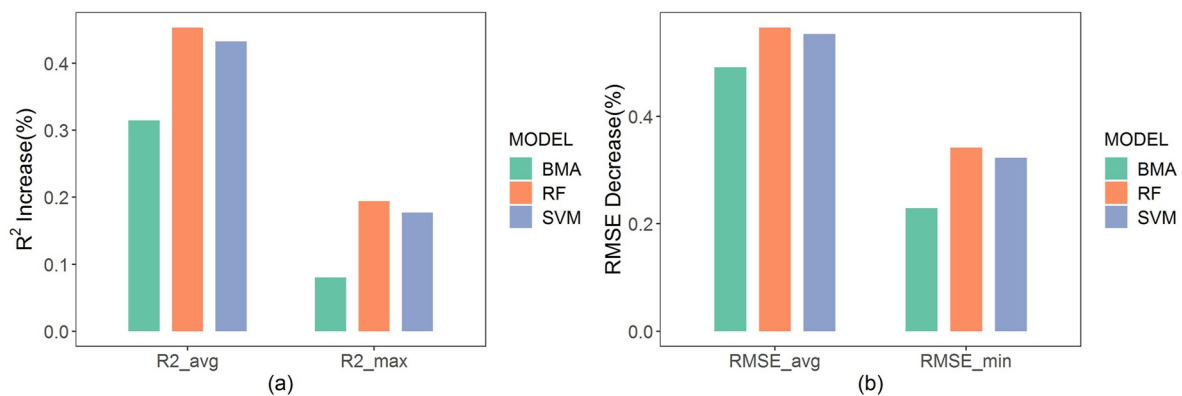

Figure 3. (a) The square of the correlation coefficients (R^2) increased percentage by BMA, RF, and SVM among the average, maximum R^2 of VPM, EC-LUE, GLO-PEM, C-Fix, and CHJ; (b) The root mean square error (RMSE) decreased percentage by BMA, RF, and SVM among the average, minimum RMSE of VPM, EC-LUE, GLO-PEM, C-Fix, and CHJ. The "R^2_avg" and the "R^2_max" represents the average and maximum of R^2, respectively. The "RMSE_avg" and the "RMSE_min" represents the average and minimum of RMSE, respectively.
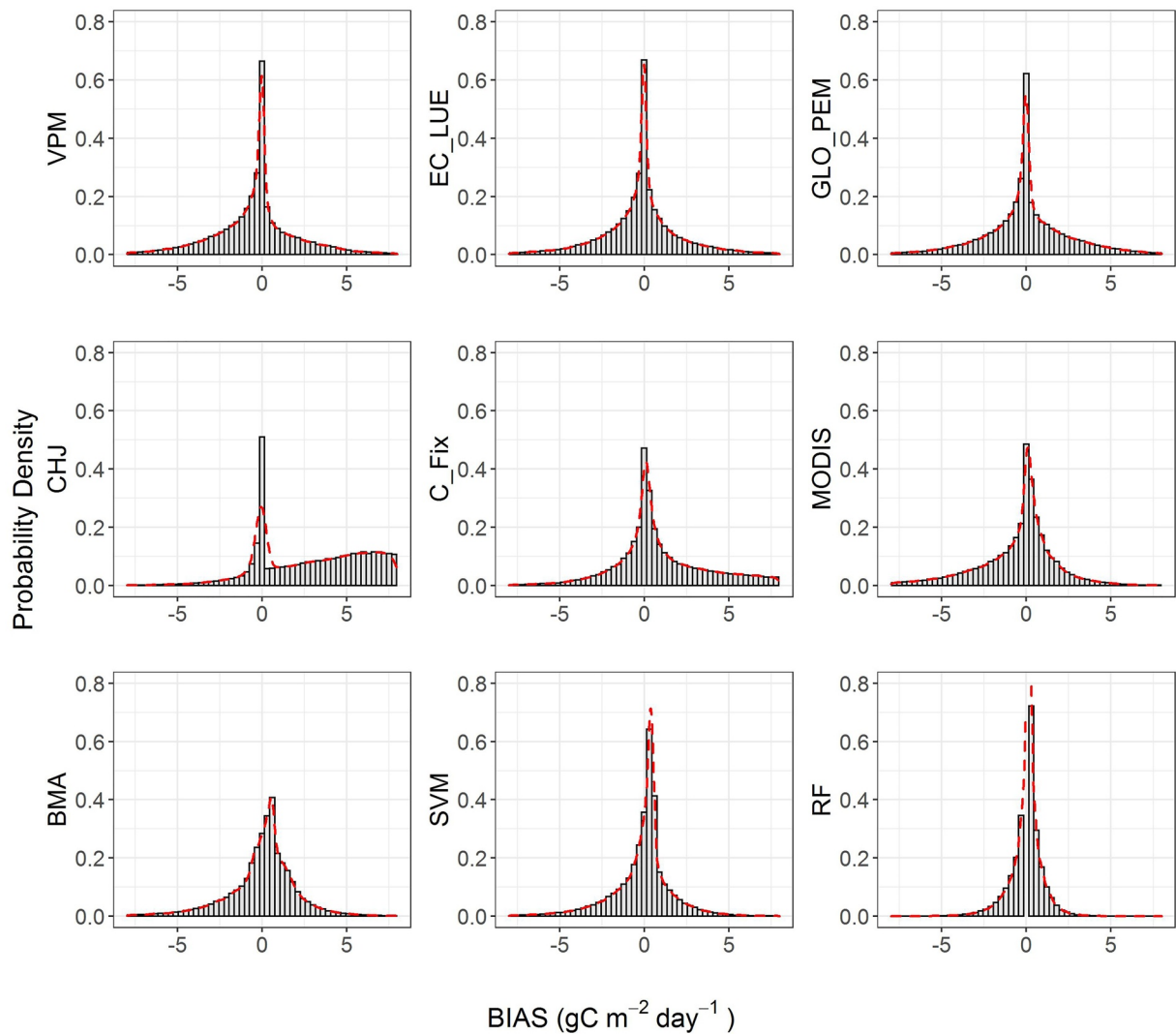
Figure 4. The probability density of predictive bias from six individual models and three fusion methods across eight ecosystem types from 56 EC flux sites.

and negative biases with a highest peak. Therefore, the histograms indicated that the RF and SVM fusion strategy can explain most of the GPP variance and conduct best performance.

The AIC and BIC values were calculated from five individual and three fusion methods across the whole data set based on Equations 26 and 27, and Table S3 in Supporting Information S1. Figure 5 showed clearly that fusion
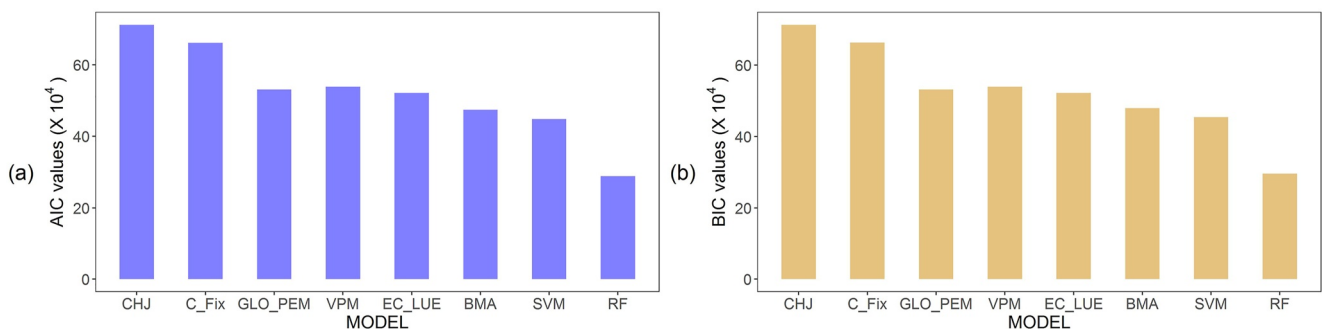

Figure 5. The (a) AIC and (b) BIC values from five individual and three fusion methods across 56 flux sites.

methods gave the lower AIC and BIC values compared to individual models. GLO-PEM, VPM and EC-LUE performed better than C-Fix and CHJ, while RF performed better than BMA and SVM. This is consistent with previous conclusions. AIC and BIC values of RF method are lower than those of SVM and BMA, and significantly lower than those of five individual models, therefore, RF represents the best GPP estimation at the 56 sites globally in this study compared with other two fusion methods and five individual models.

3.2. Comparison of the Individual and Fusion Models Based on Sites

We ran the five individual models at the 56 eddy covariance flux sites independently and ensembled them using BMA, RF, and SVM method, together with MODIS GPP product to further validate the improvement of the three fusion methods. At each site, the five-fold validation was applied to compute R^2, RMSE, and RPE for each model, reaching similar model-ranked performances as presented in Section 3.1 and in Table S2 in Supporting Information S1.

Eight representative sites in different land cover types were picked out to demonstrate the seasonal variation using the best-performing model (EC-LUE), the best fusion method (RF), and site-derived GPP. Figure 6 showed the difference between RF estimation and site-derived GPP was significantly less than that between EC-LUE and site-derived GPP, which indicated the multi-model fused method, RF, could capture more information in the seasonal variation of carbon uptake from the atmosphere compared to the best individual model, EC-LUE.

We also counted the numbers of sites for every model whose R^2 was greater than the average R^2 of all nine models (five individual models, MODIS GPP product, and three fusion models), and whose RMSE were less than the average RMSE of all models in this study. Figure 7 demonstrated that RF and SVM had higher R^2 than the average R^2 of all models at 91% of sites, and lower RMSE at 96% of sites, which indicated that at site level the fusion method of RF and SVM still performed more reliably than individual models.

4. Discussion

4.1. Performance of the Individual Models

The five individual models and the MODIS GPP product showed substantial differences in modeling daily GPP variations across eight ecosystem types at 56 EC flux sites (Tables S1 and S2 in Supporting Information S1). Among these models, EC-LUE gave the best performance considering three metrics of R^2, RMSE, and RPE over most PFTs and EC sites (Figures 1, Figure 4). First, the parameters of water stress scalar function, latent heat (LE), and sensible heat (H) were directly derived from the measurement of energy and CO_2 exchange at site scale in EC-LUE, while the water stress factor of other models came from remote sensing data or even no water stress function (C-Fix), and the spatial and temporal matching of input parameters assured the successful estimation provided by EC-LUE. Second, LE and H may be better at representing the water content and exchange between the vegetation canopy and the atmosphere for the evaporative fraction, EF, related to the surface soil water content closely, which was the major water stress on plant growth (Kurc & Small, 2004b; Zhang et al., 2015), so the EC-LUE model captured the most critical information in the photosynthesis carbon fixation processes.

VPM performed best on the Deciduous Broadleaf Forest, and quite well on Wood Savannas and other forest types because it considered the effects of leaf phenology (leaf age) on photosynthesis at the canopy level (Xiao et al., 2004, 2005). The leaf chlorophyll content and life expectancy of leaves play an important role in the light harvesting reaction during plant photosynthesis and net ecosystem exchange of carbon, especially in a deciduous forest (Croft et al., 2015; Xiao et al., 2004). The included leaf phenology scalar brings VPM extra capacity to capture the seasonal patterns of the photosynthetic process. Previous studies suggested NIR and SWIR bands are sensitive to moisture, and the water index (LSWI) derived from the combination of NIR and SWIR bands have the potential for retrieving leaf and canopy water content using remote sensing data (Ceccato et al., 2002; Xiao, 2004). The reasonable expression of water stress and plant phenology, and the easy availability of remote sensing data make VPM a popular and outstanding one in the family of LUE models.

It is well known that plant stomata would close to protect leaves from desiccation at conditions of drier air. GLO-PEM takes not only soil moisture but also air water stress (VPD) into account, which enhanced its GPP simulating ability. In this study GLO-PEM also conducted a good GPP modeling capacity over all PFTs except
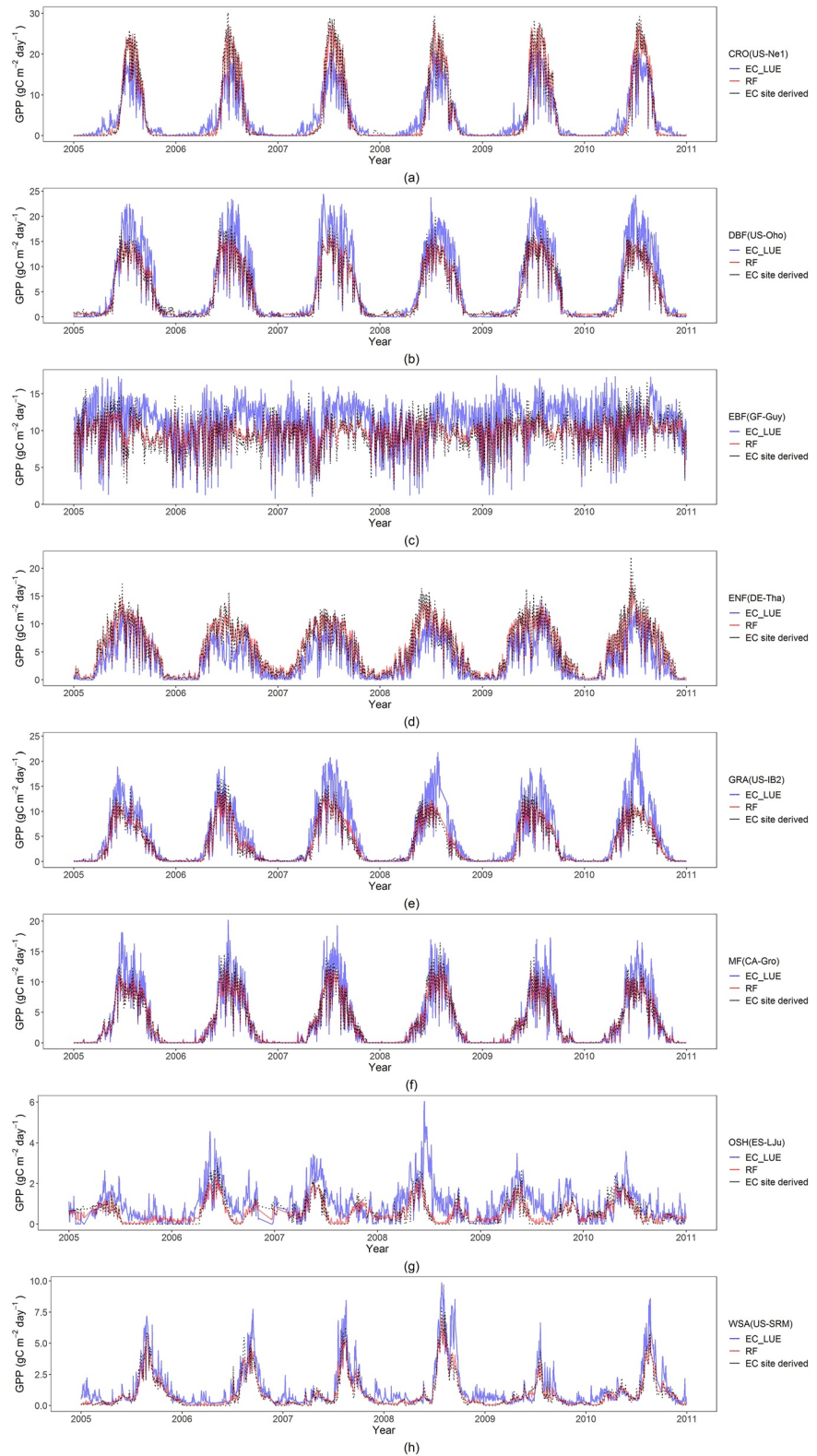
Figure 6. Examples of daily site-derived GPP (black dots), estimated GPP from the best individual model (EC-LUE, blue line) and the best fusion method (RF, orange line) for eight ecosystem types (corresponding to eight presentative EC sites): Cropland (CRO), Deciduous Broadleaf Forest (DBF), Evergreen Broadleaf Forest (EBF), Evergreen Needleleaf Forest (ENF), Mixed Forest (MF), Grassland (GRA), Open Shrublands (OSH), and Woody Savannas (WSA).
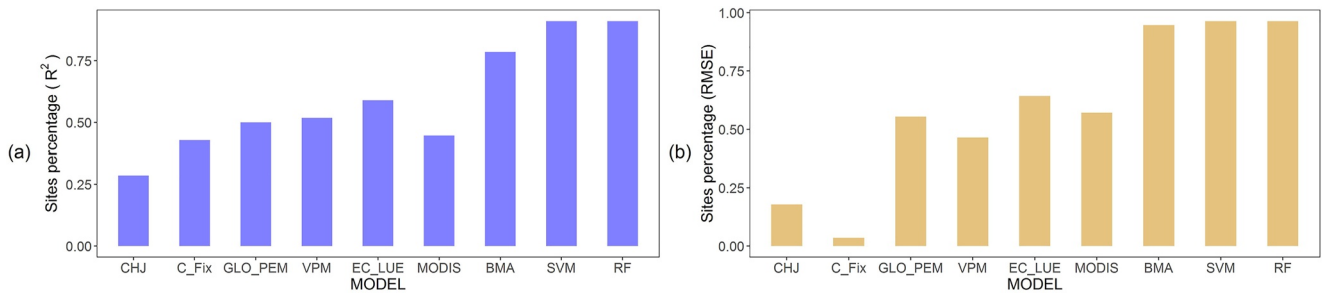
Figure 7. Percentage of sites where (a) individual model R^2 greater than average R^2 of all models and (b) individual model RMSE less than average RMSE of all models.

Open Shrublands, and it has been applied to estimate global or regional GPP using remote sensing data in many studies (Cao et al., 2004; Goetz et al., 2000).

C-Fix took CO_2 fertilization effect into the process of GPP estimation, but ignored the moisture contribution to vegetation photosynthesis, which may lead to worse model performance especially on OSH and EBF. C-Fix was developed to estimate Europe net biomass based on EC site observation and remote sensing data, and maybe not an appropriate method applied in other areas (Veroustraete et al., 1996, 2002). CHJ model ranked at the last in this study, and it performed well only on forest types except EBF. Since CHJ was proposed to simulate the global carbon sink-to-source transitions from land carbon cycle (Cox et al., 2006), it may be not suitable to estimate GPP at site scale.

4.2. Performance of the Fusion Models

We fused individual models through BMA, SVM, and RF methods, which all significantly improved the daily GPP estimation accuracy to certain degrees across eight ecosystem types at 56 EC flux sites (Figures 1–4, and Figure S1 in Supporting Information S1). The dynamic information of five GPP model processes was partially preserved in the fusion models, and we found that compared to the individual model with best performance, BMA, SVM, and RF successfully improved the estimation accuracy by 8%, 18%, and 19%, respectively. The light use efficiency model was proposed on two fundamental assumptions (Landsberg & Waring, 1997; Running et al., 2004): (a) ecosystem GPP is directly related to the absorbed photosynthetically active radiation (APAR) through LUE, which is defined as the amount of carbon fixed per unit of APAR; and (b) the actual LUE may be lower than the potential value because of the environmental stress such as water shortage and lower or higher temperature. Based on this theory, the input parameters of LUE-based GPP models derived from site measurements or remote sensing reflected the seasonal variation of plant cover information, so the individual models used in this study captured the seasonal cycle of those biomes, which contributed to the improvement of GPP estimation by fusion methods. Figure 6 showed the capacity of capturing seasonal variations using RF, the best fusion method, at eight representative sites, and the obvious improvement over EC-LUE, the best individual model, compared to site-derived GPP. Notably, as Figure 6 and Figure S1 in Supporting Information S1 showed, in contrast to other vegetation types the Evergreen Broadleaf Forest (EBF) has almost no apparent seasonal variation, therefore, the performance of individual models was abated severely (EC-LUE, $R^2 = 0.68$, RMSE = 2.91 gC m^{-2} day^{-1}, RPE = 0.08), but the three fusion methods, especially SVM and RF, still greatly increased R^2 (both being 0.80) and decreased RMSE (1.68 and 1.65 gC m^{-2} day^{-1}) and RPE (both being almost zero). The subtle changes in the seasonal leaf phenology, and various environment factors jointly increased the uncertainty of modeling plant photosynthesis in evergreen forests (Xiao et al., 2005; Yuan et al., 2014). This conclusion was consistent with previous modeling studies that LUE-based models performed the best for deciduous broadleaf sites, but not well for evergreen sites (Raczka et al., 2013; Yuan et al., 2014).

4.3. Uncertainty in Individual Models and Fusion Methods

None of the individual models achieved the best GPP prediction compared to site-derived GPP across all biomes, or at all 56 EC sites. On average, EC-LUE performed slightly better than VPM, GLO-PEM, and MODIS GPP product, while C-Fix and CHJ ranked bottom of all individual models. The reasons for uncertainty in GPP individual and fusion models could be attributed to factors such as errors from site observations, remote sensing data, and the structure of individual LUE models in this study.

The FLUXNET2015 GPP products we used to calibrate models were not directly measured but derived from direct measured NEE data. The uncertainties associated with derived-GPP data have been systematically analyzed and estimated in Pastorello et al. (2020). Here, we illustrated major type/nature of uncertainty sources associated with measurements and data processing methods, while further details can be found in Pastorello et al. (2020). Major uncertainties of derived-GPP are associated with gap-filling of data series and partitioning NEE into GPP and ecosystem respiration. Data gaps are caused mainly by instrumental failure, bad weather condition, and low turbulent data associated with advection issues (Aubinet et al., 2012; Goulden et al., 1996; Yi et al., 2005, 2008). The turbulence strength can be measured by a friction velocity (USTAR). A USTAR threshold is applied to each site, below which NEE data are treated as bad data and filled with predicted NEE by regression relationship of nighttime NEE with temperature above the USTAR threshold. FLUXNET2015 used three partitioning methods to derive GPP from NEE: nighttime fluxes method, daytime fluxes method, and sundown reference respiration (Pastorello et al., 2020). We used the derived-GPP by the daytime method because this daytime method does not treat GPP just as a difference between daytime NEE and respiration predicted by a respiration-temperature relationship obtained from nighttime data. It also includes adjustment of water stress's effect on the light-response curve. Daytime ecosystem respiration might not be the same as nighttime ecosystem respiration (Yi et al., 2004).

For the FLUXNET2015 data set, although the contributed data by regional flux nets underwent a uniform data quality control process, the energy budget is still not closed at most tower sites due to complexities in the wind patterns, footprint variability, and landscape-level heterogeneity which may lead to an error of approximately 5%–20% (Foken, 2008; Pastorello et al., 2020; Stoy et al., 2013). These errors that come from eddy covariance measurements may reduce the accuracy of individual models and further bring into the fusion methods. Some errors in the MODIS products such as FPAR and GPP employed in this study have been revealed in recent literature, and those errors also contributed to the uncertainty of accuracy in GPP prediction (Running et al., 2000; Serbin et al., 2013; Zhao et al., 2005). The spatial resolution of MODIS products was no less 500 m, which was greater than the footprint of flux site measurements that have a spatial resolution of several or tens of meters. The coarse MODIS products may capture more noise signals at corresponding sites which are at a sub-grid scale due to spatial heterogeneity, especially when these sites were located in complex terrain, so the spatial scale mismatch between remote sensing and in situ observed or derived data will introduce extra errors in GPP modeling.

The structure of individual models, especially the water stress function, was the most important source of variations among these models, and caused vastly different performance in GPP simulations (Raczka et al., 2013; Yuan et al., 2014; Zhang et al., 2015). Defining the effects of water availability on photosynthesis remains a longstanding challenge, and many water stress functions have been proposed, including as a function of VPD, soil moisture, and the ratio of actual evapotranspiration to net shortwave radiation (Cao et al., 2004; Running et al., 2000; Yuan et al., 2007). There were still controversies on which water stress factors were optimal, for example, VPD was considered as a key piece of information in the water stress expression in many studies (Zhang et al., 2015; Zhao et al., 2005), but Yuan's study indicated that VPD was not a good indicator of the spatial heterogeneity of soil moisture conditions and it is not likely to be linearly related to soil water availability (Yuan et al., 2007).

The EF used in EC-LUE was a good indicator of soil or vegetation moisture conditions because decreasing amounts of energy partitioned into latent heat flux suggests a stronger moisture limitation, but the calculation of EF needs an ET model to simulate evapotranspiration, which may introduce more errors into GPP models (Yuan et al., 2007, 2014). The satellite-derived water index (LSWI) used in VPM that can reflect the soil and vegetation moisture was easy to obtain from remote sensing data and practical to implement, but cannot reflect the air water condition because of the weak effects of atmospheric water vapor on NIR and SWIR bands (Xiao et al., 2004; Zhang et al., 2015). Previous studies have indicated that increased fraction of diffuse radiation during cloudy days enhanced plant photosynthesis, which lead to an increase of the blue or red light ratio, and diffuse radiation penetrated to lower depths of the canopy more efficiently than direct radiation (Alton et al., 2007; Gu et al., 2002; Matsuda et al., 2004), but none of the five individual models, or MODIS GPP algorithm, imported the diffuse radiation effect on photosynthesis.

The strategies to integrate temperature and water stress (multiplicative method such as VPM or minimum method such as EC-LUE) also affect the performance of simulating GPP (Zhang et al., 2015). Collectively, the errors from EC sites and remote sensing data, and the structure of individual LUE-based GPP models including definition of environmental stress functions and the strategies to integrate environmental stress, will cause the uncertainties in the individual models and further bring these uncertainties into fusion methods as input parameters.

4.4. The Performances of Individual and Fusion Models Validated by FLUXNET2015 Daytime and Nighttime GPP Products

The FLUXNET2015 data set provides GPP products based on daytime partitioning method (DT) which uses daytime and nighttime data to parameterize a model based on a light-response curve for GPP (Lasslop et al., 2010) and nighttime partitioning method (NT) which uses nighttime data to parameterize a respiration-temperature model to estimate ecosystem respiration (Reichstein et al., 2005).

The daytime method is described in Section 2 and FLUXNET2015 DT GPP products are used to validate the performance of individual and fused GPP models in this study. The complex interactions among physiological processes cannot be fully described by the light-response curve approach, so there are still some limitations in DT method (Lasslop et al., 2010). Higher assimilation rates have been observed with increasing fraction of diffuse radiation, but the diffuse effect is not reflected in DT method. Circadian rhythms of stomatal conductance, the component temperature from different parts of the ecosystem, and the quality of the NEE measurements may also introduce uncertainties in GPP estimates derived with DT method. The nighttime algorithm takes a short-term temperature response of ecosystem respiration into consideration. However, the noisiness of the eddy covariance data sabotages the reliability of the short-term relationship between respiration and temperature, and other factors such as rewetting events causing short-term dynamics of soil moisture, would also bring confounding effects in NT method (Reichstein et al., 2005).

Despite the uncertainties in partitioning CO_2 fluxes from NEE into estimates of its two main components, FULX-NET2015 DT and NT GPP products are still among the most widely used datasets for its reliability and consistency to validate estimates of GPP models, especially those of remote-sensing-based models. To further explore the impact of different partitioning algorithms on the performance of individual and fusion models, we ran the individual and fusion GPP models and evaluated them by FULXNET2015 DT product, NT product and the average of DT and NT products (DTNT) at 56 flux sites respectively.

Figure 8 showed the performance (R^2 distribution) of the five individual models, MODIS GPP product, and three fusion methods at 56 flux sites. For the five individual models, the performances evaluated by NT and
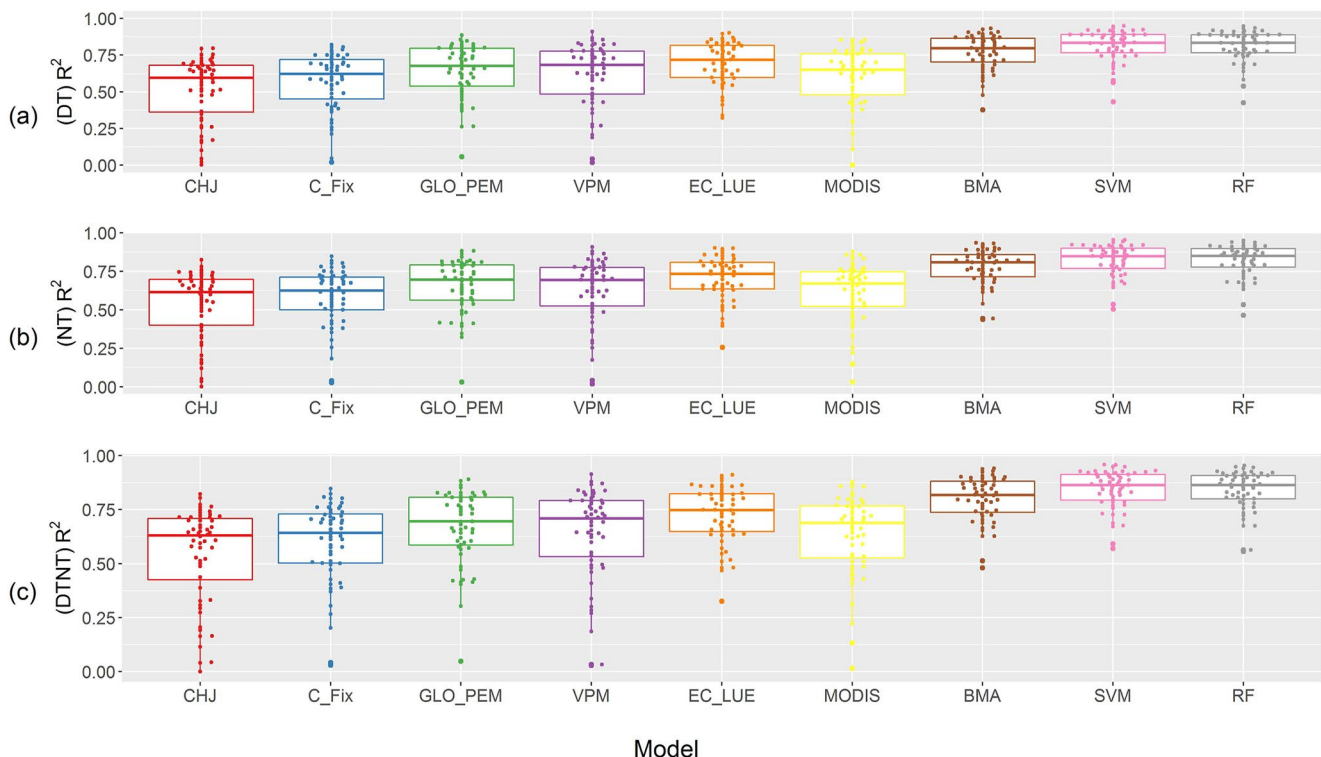

Figure 8. The performance (R^2 distribution) of the five individual models, MODIS GPP product, and three fusion models validated by FULXNET2015 daytime GPP product (DT), nighttime GPP product (NT) and the average of daytime and nighttime GPP product (DTNT) at 56 flux sites.

Table 3
The Information of 56 Sites in This Study

SITE_ID	LAT	LON	PFT	SITE_DOI	Reference
AT-Neu	47.12	11.32	GRA	10.18140/FLX/1440121	Wohlfahrt et al. (2008)
AU-How	−12.49	131.15	WSA	10.18140/FLX/1440125	Beringer et al. (2011)
AU-Tum	−35.66	148.15	EBF	10.18140/FLX/1440126	Leuning et al. (2005)
BE-Bra	51.31	4.52	MF	10.18140/FLX/1440128	Carrara et al. (2004)
BE-Lon	50.55	4.75	CRO	10.18140/FLX/1440129	Moureaux et al. (2006)
BE-Vie	50.30	6.00	MF	10.18140/FLX/1440130	Aubinet et al. (2001)
CA-Gro	48.22	−82.16	MF	10.18140/FLX/1440034	Barr et al. (2013)
CA-Oas	53.63	−106.20	DBF	10.18140/FLX/1440043	Barr et al. (2004)
CA-Obs	53.99	−105.12	ENF	10.18140/FLX/1440044	Barr et al. (2013)
CA-Qfo	49.69	−74.34	ENF	10.18140/FLX/1440045	Baldocchi & Penuelas (2019)
CA-TP1	42.66	−80.56	ENF	10.18140/FLX/1440050	Arain & Restrepo-Coupe (2005)
CA-TP3	42.71	−80.35	ENF	10.18140/FLX/1440052	Arain & Restrepo-Coupe (2005)
CA-TP4	42.71	−80.36	ENF	10.18140/FLX/1440053	Arain & Restrepo-Coupe (2005)
CH-Cha	47.21	8.41	GRA	10.18140/FLX/1440131	Merbold et al. (2014)
CH-Dav	46.82	9.86	ENF	10.18140/FLX/1440132	Zielis et al. (2014)
CH-Fru	47.12	8.54	GRA	10.18140/FLX/1440133	Imer et al. (2013)
CZ-BK1	49.50	18.54	ENF	10.18140/FLX/1440143	Acosta et al. (2013)
DE-Geb	51.10	10.91	CRO	10.18140/FLX/1440146	Anthoni et al. (2004)
DE-Gri	50.95	13.51	GRA	10.18140/FLX/1440147	Prescher et al. (2010)
DE-Hai	51.08	10.45	DBF	10.18140/FLX/1440148	Knohl et al. (2003)
DE-Kli	50.89	13.52	CRO	10.18140/FLX/1440149	Prescher et al. (2010)
DE-Tha	50.96	13.57	ENF	10.18140/FLX/1440152	Prescher et al. (2010)
DK-Sor	55.49	11.64	DBF	10.18140/FLX/1440155	Pilegaard et al. (2011)
ES-LJu	36.93	−2.75	OSH	10.18140/FLX/1440157	Serrano-Ortiz et al. (2009)
FI-Hyy	61.85	24.29	ENF	10.18140/FLX/1440158	Suni et al. (2003)
FI-Sod	67.36	26.64	ENF	10.18140/FLX/1440160	Thum et al. (2007)
FR-Fon	48.48	2.78	DBF	10.18140/FLX/1440161	Bazot et al. (2013)
FR-Gri	48.84	1.95	CRO	10.18140/FLX/1440162	Loubet et al. (2011)
FR-Pue	43.74	3.60	EBF	10.18140/FLX/1440164	Rambal et al. (2004)
GF-Guy	5.28	−52.92	EBF	10.18140/FLX/1440165	Bonal et al. (2008)
IT-BCi	40.52	14.96	CRO	10.18140/FLX/1440166	Vitale et al. (2016)
IT-Col	41.85	13.59	DBF	10.18140/FLX/1440167	Valentini et al. (2000)
IT-Lav	45.96	11.28	ENF	10.18140/FLX/1440169	Marcolla et al. (2003)
IT-MBo	46.01	11.05	GRA	10.18140/FLX/1440170	Barbara Marcolla et al. (2011)
IT-Ren	46.59	11.43	ENF	10.18140/FLX/1440173	Montagnani et al. (2009)
IT-SRo	43.73	10.28	ENF	10.18140/FLX/1440176	Chiesi et al. (2005)
NL-Hor	52.24	5.07	GRA	10.18140/FLX/1440177	Jacobs et al. (2007)
NL-Loo	52.17	5.74	ENF	10.18140/FLX/1440178	Moors (2012)
RU-Cok	70.83	147.49	OSH	10.18140/FLX/1440182	van der Molen et al. (2007)
RU-Fyo	56.46	32.92	ENF	10.18140/FLX/1440183	Kurbatova et al. (2008)
US-ARM	36.61	−97.49	CRO	10.18140/FLX/1440066	Biraud et al. (2022)
US-GLE	41.37	−106.24	ENF	10.18140/FLX/1440069	Frank and Massman (2022)
US-Ha1	42.54	−72.17	DBF	10.18140/FLX/1440071	Munger (2022)

Table 3
Continued

SITE_ID	LAT	LON	PFT	SITE_DOI	Reference
US-IB2	41.84	−88.24	GRA	10.18140/FLX/1440072	Matamala (2019)
US-Me2	44.45	−121.56	ENF	10.18140/FLX/1440079	Law (2022)
US-MMS	39.32	−86.41	DBF	10.18140/FLX/1440083	Novick and Phillips (2022)
US-Ne1	41.17	−96.48	CRO	10.18140/FLX/1440084	Suyker (2022c)
US-Ne2	41.16	−96.47	CRO	10.18140/FLX/1440085	Suyker (2022a)
US-Ne3	41.18	−96.44	CRO	10.18140/FLX/1440086	Suyker (2022b)
US-NR1	40.03	−105.55	ENF	10.18140/FLX/1440087	Blanken et al. (2022)
US-Oho	41.55	−83.84	DBF	10.18140/FLX/1440088	Chen et al. (2021)
US-SRM	31.82	−110.87	WSA	10.18140/FLX/1440090	Scott (2022a)
US-Ton	38.43	−120.97	WSA	10.18140/FLX/1440092	Ma et al. (2022a)
US-UMB	45.56	−84.71	DBF	10.18140/FLX/1440093	Gough et al. (2022)
US-Var	38.41	−120.95	GRA	10.18140/FLX/1440094	Ma et al. (2022b)
US-Wkg	31.74	−109.94	GRA	10.18140/FLX/1440096	Scott (2022b)

DTNT were consistent with those by DT: EC-LUE, VPM and GLO-PEM performed better than C-Fix and CHJ. For the three fused models, the R^2 distribution evaluated by DT were all narrowly concentrated around higher values than those of individual models, with RF having the highest R^2, and then SVM, followed by BMA (shown in Panel (a) of Figure 8). The same pattern repeated when evaluated by NT and DTNT GPP products (shown in Panel (a) and (b) of Figure 8). Compared to individual models, three fusion methods visibly improved the performance of GPP estimates validated by NT and DTNT as using DT GPP products, which showed that the fusion methods could enhance the performance of GPP estimation. We also calculated RMSE and its distribution using DT, NT and DTNT products respectively, shown in Figure S2 in Supporting Information S1, which had derived the similar conclusions. The performance evaluations using FLUXNET2015 DT, NT and DTNT GPP products indicated that fusion models consistently provide a better performance in simulating ecosystem GPP than single models.

5. Conclusions

We ran five individual models (VPM, EC-LUE, GLO-PEM, CHJ, C-Fix) using eddy covariance flux data from 56 sites in FLUXNET 2015 data set and remote sensing data (MODIS reflectance and FPAR products) as input parameters, and fused them together by the methods of BMA, SVM, and RF to simulate GPP across diverse ecosystem types. For individual models, EC-LUE showed the highest correlations between modeled GPP and GPP derived from eddy covariance observations at the daily scale, and showed a better performance to capture interannual variability of GPP than other models, followed by VPM and GLO-PEM, while CHJ and C-Fix showed some limitations on the estimation accuracy. The fusion method of BMA, SVM, and RF were examined by a five-fold cross validation for each PFT, and successfully improved the estimation accuracy by 8%, 18%, and 19%, respectively. RF fusion method captured more magnitudes of site GPP measurements than SVM, BMA, and individual models. This study suggests that although the errors from different data sources and the differences between individual LUE-based GPP model structures may lead to great uncertainty in modeling GPP, machine learning methods such as RF could be an effective option to improve GPP estimation when the ability of an individual model is limited under current site conditions.

Data Availability Statement

MODIS data were obtained from https://modis.ornl.gov/. ISLSCP II data were obtained from https://doi.org/10.3334/ORNLDAAC/932. FLUXNET2015 data set was obtained from https://fluxnet.org/data/fluxnet2015-dataset/. The codes for GPP modeling and fusing are available at https://doi.org/10.5281/zenodo.7589870. The detailed information of 56 sites were listed in Table 3.

References

Acosta, M., Pavelka, M., Montagnani, L., Kutsch, W., Lindroth, A., Juszczak, R., & Janouš, D. (2013). Soil surface CO2 efflux measurements in Norway spruce forests: Comparison between four different sites across Europe — From boreal to alpine forest. *Geoderma*, *192*, 295–303. https://doi.org/10.1016/j.geoderma.2012.08.027

Akaike, H. (1974). A new look at the statistical model identification. *IEEE Transactions on Automatic Control*, *19*(6), 716–723. https://doi.org/10.1109/TAC.1974.1100705

Alton, P. B., North, P. R., & Los, S. O. (2007). The impact of diffuse sunlight on canopy light-use efficiency, gross photosynthetic product and net ecosystem exchange in three forest biomes. *Global Change Biology*, *13*(4), 776–787. https://doi.org/10.1111/j.1365-2486.2007.01316.x

Amini, S., Saber, M., Rabiei-Dastjerdi, H., & Homayouni, S. (2022). Urban land use and land cover change analysis using random forest classification of landsat time series. *Remote Sensing*, *14*(11), 2654. https://doi.org/10.3390/rs14112654

Anthoni, P. M., Knohl, A., Rebmann, C., Freibauer, A., Mund, M., Ziegler, W., et al. (2004). Forest and agricultural land-use-dependent CO2 exchange in Thuringia, Germany: Forest and agricultural CO_2 exchange. *Global Change Biology*, *10*(12), 2005–2019. https://doi.org/10.1111/j.1365-2486.2004.00863.x

Arain, M. A., & Restrepo-Coupe, N. (2005). Net ecosystem production in a temperate pine plantation in southeastern Canada. *Agricultural and Forest Meteorology*, *128*(3), 223–241. https://doi.org/10.1016/j.agrformet.2004.10.003

Aubinet, M., Chermanne, B., Vandenhaute, M., Longdoz, B., Yernaux, M., & Laitat, E. (2001). Long term carbon dioxide exchange above a mixed forest in the Belgian Ardennes. *Agricultural and Forest Meteorology*, *108*(4), 293–315. https://doi.org/10.1016/S0168-1923(01)00244-1

Aubinet, M., Vesala, T., & Papale, D. (Eds.), (2012). *Eddy covariance: A practical guide to measurement and data analysis*. Springer Netherlands. https://doi.org/10.1007/978-94-007-2351-1

Baldocchi, D., & Penuelas, J. (2019). The physics and ecology of mining carbon dioxide from the atmosphere by ecosystems. *Global Change Biology*, *25*(4), 1191–1197. https://doi.org/10.1111/gcb.14559

Barr, A. G., Black, T. A., Hogg, E. H., Kljun, N., Morgenstern, K., & Nesic, Z. (2004). Inter-annual variability in the leaf area index of a boreal aspen-hazelnut forest in relation to net ecosystem production. *Agricultural and Forest Meteorology*, *126*(3), 237–255. https://doi.org/10.1016/j.agrformet.2004.06.011

Barr, A. G., Richardson, A. D., Hollinger, D. Y., Papale, D., Arain, M. A., Black, T. A., et al. (2013). Use of change-point detection for friction–velocity threshold evaluation in eddy-covariance studies. *Agricultural and Forest Meteorology*, *171–172*, 31–45. https://doi.org/10.1016/j.agrformet.2012.11.023

Bazot, S., Barthes, L., Blanot, D., & Fresneau, C. (2013). Distribution of non-structural nitrogen and carbohydrate compounds in mature oak trees in a temperate forest at four key phenological stages. *Trees*, *27*(4), 1023–1034. https://doi.org/10.1007/s00468-013-0853-5

Beringer, J., Hacker, J., Hutley, L. B., Leuning, R., Arndt, S. K., Amiri, R., et al. (2011). SPECIAL—Savanna patterns of energy and carbon integrated across the landscape. *Bulletin of the American Meteorological Society*, *92*(11), 1467–1485. https://doi.org/10.1175/2011BAMS2948.1

Biraud, S., Fischer, M., Chan, S., & Torn, M. (2022). AmeriFlux FLUXNET-1F US-ARM ARM southern great plains site- lamont, Ver. 3-5 (Dataset). *AmeriFlux AMP*. https://doi.org/10.17190/AMF/1854366

Blanken, P. D., Monson, R. K., Burns, S. P., Bowling, D. R., & Turnipseed, A. A. (2022). AmeriFlux FLUXNET-1F US-NR1 Niwot ridge forest (LTER NWT1), Ver. 3-5 (Dataset). *AmeriFlux AMP*. https://doi.org/10.17190/AMF/1871141

Bonal, D., Bosc, A., Ponton, S., Goret, J.-Y., Burban, B., Gross, P., et al. (2008). Impact of severe dry season on net ecosystem exchange in the neotropical rainforest of French Guiana: Higher nep under severe drought. *Global Change Biology*, *14*(8), 1917–1933. https://doi.org/10.1111/j.1365-2486.2008.01610.x

Breiman, L. (2001). Random forests. *Machine Learning*, *45*(1), 5–32. https://doi.org/10.1023/A:1010933404324

Canadell, J. G., Mooney, H. A., Baldocchi, D. D., Berry, J. A., Ehleringer, J. R., Field, C. B., et al. (2000). Carbon metabolism of the terrestrial biosphere: A multitechnique approach for improved understanding. *Ecosystems*, *3*(2), 115–130. https://doi.org/10.1007/s100210000014

Cao, M., Prince, S. D., Small, J., & Goetz, S. J. (2004). Remotely sensed interannual variations and trends in terrestrial net primary productivity 1981-2000. *Ecosystems*, *7*(3), 233–242. https://doi.org/10.1007/s10021-003-0189-x

Carrara, A., Janssens, I. A., Curiel Yuste, J., & Ceulemans, R. (2004). Seasonal changes in photosynthesis, respiration and NEE of a mixed temperate forest. *Agricultural and Forest Meteorology*, *126*(1), 15–31. https://doi.org/10.1016/j.agrformet.2004.05.002

Ceccato, P., Gobron, N., Flasse, S., Pinty, B., & Tarantola, S. (2002). Designing a spectral index to estimate vegetation water content from remote sensing data: Part 1. theoretical approach. *Remote Sensing of Environment*, *10*.

Chen, J., Chu, H., & Noormets, A. (2021). AmeriFlux BASE US-Oho Oak openings, Ver. 7-5 (Dataset). *AmeriFlux AMP*. https://doi.org/10.17190/AMF/1246089

Chen, Y., Yuan, W., Xia, J., Fisher, J. B., Dong, W., Zhang, X., et al. (2015). Using Bayesian model averaging to estimate terrestrial evapotranspiration in China. *Journal of Hydrology*, *528*, 537–549. https://doi.org/10.1016/j.jhydrol.2015.06.059

Chiesi, M., Maselli, F., Bindi, M., Fibbi, L., Cherubini, P., Arlotta, E., et al. (2005). Modelling carbon budget of Mediterranean forests using ground and remote sensing measurements. *Agricultural and Forest Meteorology*, *135*(1–4), 22–34. https://doi.org/10.1016/j.agrformet.2005.09.011

Cortes, C., & Vapnik, V. (1995). Support-vector networks. *Machine Learning*, *20*(3), 273–297. https://doi.org/10.1007/BF00994018

Cox, P., Huntingford, C., & Jones, C. (2006). *Conditions for sink-to-source transitions and runaway feedbacks from the land carbon cycle* (pp. 155–162). Cambridge University Press.

Cox, P. M., Betts, R. A., Jones, C. D., Spall, S. A., & Totterdell, I. J. (2000). Acceleration of global warming due to carbon-cycle feedbacks in a coupled climate model. *Nature*, *408*(6809), 184–187. https://doi.org/10.1038/35041539

Crisp, D., Dolman, H., Tanhua, T., McKinley, G. A., Hauck, J., Bastos, A., et al. (2022). How well do we understand the land-ocean-atmosphere carbon cycle? *Reviews of Geophysics*, *60*(2). https://doi.org/10.1029/2021RG000736

Croft, H., Chen, J. M., Froelich, N. J., Chen, B., & Staebler, R. M. (2015). Seasonal controls of canopy chlorophyll content on forest carbon uptake: Implications for GPP modeling. *Journal of Geophysical Research: Biogeosciences*, *120*(8), 1576–1586. https://doi.org/10.1002/2015JG002980

Cui, Y., Xiao, X., Zhang, Y., Dong, J., Qin, Y., Doughty, R. B., et al. (2017). Temporal consistency between gross primary production and solar-induced chlorophyll fluorescence in the ten most populous megacity areas over years. *Scientific Reports*, *7*(1), 14963. https://doi.org/10.1038/s41598-017-13783-5

Duan, Q., & Phillips, T. J. (2010). Bayesian estimation of local signal and noise in multimodel simulations of climate change. *Journal of Geophysical Research*, *115*(D18), D18123. https://doi.org/10.1029/2009JD013654

Foken, T. (2008). The energy balance closure problem: An overview. *Ecological Applications*, *18*(6), 1351–1367. https://doi.org/10.1890/06-0922.1

Frank, J., & Massman, B. (2022). AmeriFlux FLUXNET-1F US-GLE GLEES, Ver. 3-5 (Dataset). *AmeriFlux AMP*. https://doi.org/10.17190/AMF/1871136

Goetz, S. J., Prince, S. D., Small, J., & Gleason, A. C. R. (2000). Interannual variability of global terrestrial primary production: Results of a model driven with satellite observations. *Journal of Geophysical Research*, *105*(D15), 20077–20091. https://doi.org/10.1029/2000JD900274

Gough, C., Bohrer, G., & Curtis, P. (2022). AmeriFlux BASE US-UMB University of Mich. Biological station, Ver. 18-5 (Dataset). *AmeriFlux AMP*. https://doi.org/10.17190/AMF/1246107

Goulden, M. L., Munger, J. W., Fan, S.-M., Daube, B. C., & Wofsy, S. C. (1996). Measurements of carbon sequestration by long-term eddy covariance: Methods and a critical evaluation of accuracy. *Global Change Biology*, *2*(3), 169–182. https://doi.org/10.1111/j.1365-2486.1996.tb00070.x

Gu, L., Baldocchi, D., Verma, S. B., Black, T. A., Vesala, T., Falge, E. M., & Dowty, P. R. (2002). Advantages of diffuse radiation for terrestrial ecosystem productivity. *Journal of Geophysical Research*, *107*(D6), ACL2-1–ACL2-23. https://doi.org/10.1029/2001JD001242

Gyamerah, S., Ngare, P., & Ikpe, D. (2020). Probabilistic forecasting of crop yields via quantile random forest and Epanechnikov Kernel function. *Agricultural and Forest Meteorology*, *280*, 107808. https://doi.org/10.1016/j.agrformet.2019.107808

Imer, D., Merbold, L., Eugster, W., & Buchmann, N. (2013). Temporal and spatial variations of soil CO_2, CH_4, and N_2O fluxes at three differently managed grasslands. *Biogeosciences*, *10*(9), 5931–5945. https://doi.org/10.5194/bg-10-5931-2013

Jacobs, C. M. J., Jacobs, A. F. G., Bosveld, F. C., Hendriks, D. M. D., Hensen, A., Kroon, P. S., et al. (2007). Variability of annual CO_2 exchange from Dutch grasslands. *Biogeosciences*, *4*(5), 803–816. https://doi.org/10.5194/bg-4-803-2007

Keenan, T. F., Baker, I., Barr, A., Ciais, P., Davis, K., Dietze, M., et al. (2012). Terrestrial biosphere model performance for inter-annual variability of land-atmosphere CO_2 exchange. *Global Change Biology*, *18*(6), 1971–1987. https://doi.org/10.1111/j.1365-2486.2012.02678.x

Khalil, A. F., McKee, M., Kemblowski, M., Asefa, T., & Bastidas, L. (2006). Multiobjective analysis of chaotic dynamic systems with sparse learning machines. *Advances in Water Resources*, *29*(1), 72–88. https://doi.org/10.1016/j.advwatres.2005.05.011

Knohl, A., Schulze, E.-D., Kolle, O., & Buchmann, N. (2003). Large carbon uptake by an unmanaged 250-year-old deciduous forest in Central Germany. *Agricultural and Forest Meteorology*, *118*(3–4), 151–167. https://doi.org/10.1016/S0168-1923(03)00115-1

Kurbatova, J., Li, C., Varlagin, A., Xiao, X., & Vygodskaya, N. (2008). Modeling carbon dynamics in two adjacent spruce forests with different soil conditions in Russia. *Biogeosciences*, *5*(4), 969–980. https://doi.org/10.5194/bg-5-969-2008

Kurc, S. A., & Small, E. E. (2004a). Dynamics of evapotranspiration in semiarid grassland and shrubland ecosystems during the summer monsoon season, central New Mexico. *Water Resources Research*, *40*(9). https://doi.org/10.1029/2004WR003068

Kurc, S. A., & Small, E. E. (2004b). Dynamics of evapotranspiration in semiarid grassland and shrubland ecosystems during the summer monsoon season (Vol. *15*).

Landsberg, J. J., & Waring, R. H. (1997). A generalised model of forest productivity using simplified concepts of radiation-use efficiency, carbon balance and partitioning. *Forest Ecology and Management*, *95*(3), 209–228. https://doi.org/10.1016/S0378-1127(97)00026-1

Lasslop, G., Reichstein, M., Papale, D., Richardson, A. D., Arneth, A., Barr, A., et al. (2010). Separation of net ecosystem exchange into assimilation and respiration using a light response curve approach: Critical issues and global evaluation: Separation of NEE into GPP and RECO. *Global Change Biology*, *16*(1), 187–208. https://doi.org/10.1111/j.1365-2486.2009.02041.x

Law, B. (2022). AmeriFlux BASE US-Me2 Metolius mature ponderosa pine, Ver. 18-5 (Dataset). *AmeriFlux AMP*. https://doi.org/10.17190/AMF/1246076

Leuning, R., Cleugh, H. A., Zegelin, S. J., & Hughes, D. (2005). Carbon and water fluxes over a temperate Eucalyptus forest and a tropical wet/dry savanna in Australia: Measurements and comparison with MODIS remote sensing estimates. *Agricultural and Forest Meteorology*, *129*(3), 151–173. https://doi.org/10.1016/j.agrformet.2004.12.004

Lewis, J. M. (1995). The story behind the Bowen ratio. *Bulletin of the American Meteorological Society*, *76*(12), 2433–2443. https://doi.org/10.1175/1520-0477(1995)076<2433:TSBTBR>2.0.CO;2

Li, X., Liang, S., Yu, G., Yuan, W., Cheng, X., Xia, J., et al. (2013). Estimation of gross primary production over the terrestrial ecosystems in China. *Ecological Modelling*, *261–262*, 80–92. https://doi.org/10.1016/j.ecolmodel.2013.03.024

Liang, S., Zhao, X., Liu, S., Yuan, W., Cheng, X., Xiao, Z., et al. (2013). A long-term Global LAnd Surface Satellite (GLASS) data-set for environmental studies. *International Journal of Digital Earth*, *6*(1), 5–33. https://doi.org/10.1080/17538947.2013.805262

Liaw, A., & Wiener, M. (2002). Classification and regression by randomForest. *R News*, *2*, 18–22.

Loubet, B., Laville, P., Lehuger, S., Larmanou, E., Flechard, C., Mascher, N., et al. (2011). Carbon, nitrogen and Greenhouse gases budgets over a four years crop rotation in northern France. *Plant and Soil*, *343*(1–2), 109–137. https://doi.org/10.1007/s11104-011-0751-9

Ma, S., Xu, L., Verfaillie, J., & Baldocchi, D. (2022a). AmeriFlux BASE US-Ton Tonzi Ranch, Ver. 16-5 (Dataset). *AmeriFlux AMP*. https://doi.org/10.17190/AMF/1245971

Ma, S., Xu, L., Verfaillie, J., & Baldocchi, D. (2022b). AmeriFlux BASE US-Var Vaira Ranch- Ione, Ver. 18-5 (Dataset). *AmeriFlux AMP*. https://doi.org/10.17190/AMF/1245984

Marcolla, B., Cescatti, A., Manca, G., Zorer, R., Cavagna, M., Fiora, A., et al. (2011). Climatic controls and ecosystem responses drive the inter-annual variability of the net ecosystem exchange of an alpine meadow. *Agricultural and Forest Meteorology*, *151*(9), 1233–1243. https://doi.org/10.1016/j.agrformet.2011.04.015

Marcolla, B., Pitacco, A., & Cescatti, A. (2003). Canopy architecture and turbulence structure in a coniferous forest. *Boundary-Layer Meteorology*, *108*(1), 39–59. https://doi.org/10.1023/A:1023027709805

Matamala, R. (2019). AmeriFlux BASE US-IB2 Fermi national accelerator laboratory- Batavia (Prairie site), Ver. 8-5 (Dataset). *AmeriFlux AMP*. https://doi.org/10.17190/AMF/1246066

Matsuda, R., Ohashi-Kaneko, K., Fujiwara, K., Goto, E., & Kurata, K. (2004). Photosynthetic characteristics of rice leaves grown under red light with or without supplemental blue light. *Plant and Cell Physiology*, *45*(12), 1870–1874. https://doi.org/10.1093/pcp/pch203

Meng, Y., Yang, M., Liu, S., Mou, Y., Peng, C., & Zhou, X. (2021). Quantitative assessment of the importance of bio-physical drivers of land cover change based on a random forest method. *Ecological Informatics*, *61*, 101204. https://doi.org/10.1016/j.ecoinf.2020.101204

Merbold, L., Eugster, W., Stieger, J., Zahniser, M., Nelson, D., & Buchmann, N. (2014). Greenhouse gas budget (CO_2, CH_4 and N_2O) of intensively managed grassland following restoration. *Global Change Biology*, *20*(6), 1913–1928. https://doi.org/10.1111/gcb.12518

Montagnani, L., Manca, G., Canepa, E., Georgieva, E., Acosta, M., Feigenwinter, C., et al. (2009). A new mass conservation approach to the study of CO_2 advection in an alpine forest. *Journal of Geophysical Research*, *114*(D7), D07306. https://doi.org/10.1029/2008JD010650

Monteith, J. L. (1972). Solar radiation and productivity in tropical ecosystems. *Journal of Applied Ecology*, *9*(3), 747. https://doi.org/10.2307/2401901

Moors, E. J. (2012). *Water use of forests in The Netherlands* (p. 292). Vrije Universiteit Amsterdam.

Moureaux, C., Debacq, A., Bodson, B., Heinesch, B., & Aubinet, M. (2006). Annual net ecosystem carbon exchange by a sugar beet crop. *Agricultural and Forest Meteorology*, *139*(1), 25–39. https://doi.org/10.1016/j.agrformet.2006.05.009

Munger, J. W. (2022). AmeriFlux FLUXNET-1F US-Ha1 Harvard forest EMS tower (HFR1), Ver. 3-5 (Dataset). *AmeriFlux AMP*. https://doi.org/10.17190/AMF/1871137

Nemani, R. R., Keeling, C. D., Hashimoto, H., Jolly, W. M., Piper, S. C., Tucker, C. J., et al. (2003). Climate-driven increases in global terrestrial net primary production from 1982 to 1999. *Science*, *300*(5625), 1560–1563. https://doi.org/10.1126/science.1082750

Novick, K., & Phillips, R. (2022). AmeriFlux FLUXNET-1F US-MMS Morgan Monroe state forest, Ver. 3-5 (Dataset). *AmeriFlux AMP*. https://doi.org/10.17190/AMF/1854369

Pastorello, G., Trotta, C., Canfora, E., Chu, H., Christianson, D., Cheah, Y.-W., et al. (2020). The FLUXNET2015 dataset and the ONEFlux processing pipeline for eddy covariance data. *Scientific Data*, *7*(1), 225. https://doi.org/10.1038/s41597-020-0534-3

Pei, Y., Dong, J., Zhang, Y., Yuan, W., Doughty, R., Yang, J., et al. (2022). Evolution of light use efficiency models: Improvement, uncertainties, and implications. *Agricultural and Forest Meteorology*, *317*, 108905. https://doi.org/10.1016/j.agrformet.2022.108905

Pilegaard, K., Ibrom, A., Courtney, M. S., Hummelshøj, P., & Jensen, N. O. (2011). Increasing net CO_2 uptake by a Danish beech forest during the period from 1996 to 2009. *Agricultural and Forest Meteorology*, *151*(7), 934–946. https://doi.org/10.1016/j.agrformet.2011.02.013

Potter, C. S., Randerson, J. T., Field, C. B., Matson, P. A., Vitousek, P. M., Mooney, H. A., & Klooster, S. A. (1993). Terrestrial ecosystem production: A process model based on global satellite and surface data. *Global Biogeochemical Cycles*, *7*(4), 811–841. https://doi.org/10.1029/93GB02725

Prescher, A.-K., Grünwald, T., & Bernhofer, C. (2010). Land use regulates carbon budgets in eastern Germany: From NEE to NBP. *Agricultural and Forest Meteorology*, *150*(7), 1016–1025. https://doi.org/10.1016/j.agrformet.2010.03.008

Priestley, C. H. B., & Taylor, R. J. (1972). On the assessment of surface heat flux and evaporation using large-scale parameters. *Monthly Weather Review*, *100*(2), 81–92. https://doi.org/10.1175/1520-0493(1972)100<0081:OTAOSH>2.3.CO;2

Prince, S. D., & Goward, S. N. (1995). Global primary production: A remote sensing approach. *Journal of Biogeography*, *22*(4/5), 815–835. https://doi.org/10.2307/2845983

Raczka, B. M., Davis, K. J., Huntzinger, D., Neilson, R. P., Poulter, B., Richardson, A. D., et al. (2013). Evaluation of continental carbon cycle simulations with North American flux tower observations. *Ecological Monographs*, *83*(4), 531–556. https://doi.org/10.1890/12-0893.1

Raftery, A. E., Gneiting, T., Balabdaoui, F., & Polakowski, M. (2005). Using Bayesian model averaging to calibrate forecast ensembles. *Monthly Weather Review*, *133*(5), 1155–1174. https://doi.org/10.1175/MWR2906.1

Raich, J. W., Rastetter, E. B., Melillo, J. M., Kicklighter, D. W., Steudler, P. A., Peterson, B. J., et al. (1991). Potential net primary productivity in South America: Application of a global model. *Ecological Applications*, *1*(4), 399–429. https://doi.org/10.2307/1941899

Rambal, S., Joffre, R., Ourcival, J. M., Cavender-Bares, J., & Rocheteau, A. (2004). The growth respiration component in eddy CO_2 flux from a *Quercus ilex* mediterranean forest: Growth respiration from a forest. *Global Change Biology*, *10*(9), 1460–1469. https://doi.org/10.1111/j.1365-2486.2004.00819.x

Reichstein, M., Falge, E., Baldocchi, D., Papale, D., Aubinet, M., Berbigier, P., et al. (2005). On the separation of net ecosystem exchange into assimilation and ecosystem respiration: Review and improved algorithm. *Global Change Biology*, *11*(9), 1424–1439. https://doi.org/10.1111/j.1365-2486.2005.001002.x

Running, S., Nemani, R. R., Heinsch, F. A., Zhao, M., Reeves, M., & Hashimoto, H. (2004). A continuous satellite-derived measure of global terrestrial primary production. *BioScience*, *54*(6), 547. https://doi.org/10.1641/0006-3568(2004)054[0547:ACSMOG]2.0.CO;2

Running, S., Thornton, P., Nemani, R., & Glassy, J. (2000). Global terrestrial gross and net primary productivity from the Earth observing system. *Methods in Ecosystem Science*, 44–57. https://doi.org/10.1007/978-1-4612-1224-9_4

Schwarz, G. (1978). Estimating the dimension of a model. *Annals of Statistics*, *6*(2), 461–464. https://doi.org/10.1214/aos/1176344136

Scott, R. (2022a). AmeriFlux BASE US-SRM Santa Rita Mesquite, Ver. 24-5 (Dataset). *AmeriFlux AMP*. https://doi.org/10.17190/AMF/1246104

Scott, R. (2022b). AmeriFlux BASE US-Wkg Walnut Gulch Kendall grasslands, Ver. 19-5 (Dataset). *AmeriFlux AMP*. https://doi.org/10.17190/AMF/1246112

Serbin, S. P., Ahl, D. E., & Gower, S. T. (2013). Spatial and temporal validation of the MODIS LAI and FPAR products across a boreal forest wildfire chronosequence. *Remote Sensing of Environment*, *133*, 71–84. https://doi.org/10.1016/j.rse.2013.01.022

Serrano-Ortiz, P., Domingo, F., Cazorla, A., Were, A., Cuezva, S., Villagarcía, L., et al. (2009). Interannual CO2 exchange of a sparse Mediterranean shrubland on a carbonaceous substrate. *Journal of Geophysical Research*, *114*(G4), G04015. https://doi.org/10.1029/2009JG000983

Sims, D. A., Rahman, A., Cordova, V., Elmasri, B., Baldocchi, D., Bolstad, P., et al. (2008). A new model of gross primary productivity for North American ecosystems based solely on the enhanced vegetation index and land surface temperature from MODIS. *Remote Sensing of Environment*, *112*(4), 1633–1646. https://doi.org/10.1016/j.rse.2007.08.004

Sims, D. A., Rahman, A. F., Cordova, V. D., El-Masri, B. Z., Baldocchi, D. D., Flanagan, L. B., et al. (2006). On the use of MODIS EVI to assess gross primary productivity of North American ecosystems. *Journal of Geophysical Research*, *111*(G4). https://doi.org/10.1029/2006JG000162

Stoy, P. C., Mauder, M., Foken, T., Marcolla, B., Boegh, E., Ibrom, A., et al. (2013). A data-driven analysis of energy balance closure across FLUXNET research sites: The role of landscape scale heterogeneity. *Agricultural and Forest Meteorology*, *171–172*, 137–152. https://doi.org/10.1016/j.agrformet.2012.11.004

Suleiman, A., & Crago, R. (2004). Hourly and daytime evapotranspiration from grassland using radiometric surface temperatures. *Agronomy Journal*, *96*(2), 384–390. https://doi.org/10.2134/agronj2004.3840

Suni, T., Rinne, J., Reissell, Ä., Altimir, N., Keronen, P., Rannik, Ü., et al. (2003). Long-term measurements of surface fluxes above a Scots pine forest in Hyytiälä, southern Finland, 1996–200, *8*, 16.

Suykens, J. A. K. (2001). Support vector machines: A nonlinear modelling and control perspective. *European Journal of Control*, *7*(2), 311–327. https://doi.org/10.3166/ejc.7.311-327

Suyker, A. (2022a). AmeriFlux BASE US-Ne2 Mead - Irrigated maize-soybean rotation site, Ver. 13-5 (Dataset). *AmeriFlux AMP*. https://doi.org/10.17190/AMF/1246085

Suyker, A. (2022b). AmeriFlux BASE US-Ne3 Mead - Rainfed maize-soybean rotation site, Ver. 13-5 (Dataset). *AmeriFlux AMP*. https://doi.org/10.17190/AMF/1246086

Suyker, A. (2022c). AmeriFlux FLUXNET-1F US-Ne1 Mead - Irrigated continuous maize site, Ver. 3-5 (Dataset). *AmeriFlux AMP*. https://doi.org/10.17190/AMF/1871140

Thum, T., Aalto, T., Laurila, T., Aurela, M., Kolari, P., & Hari, P. (2007). Parametrization of two photosynthesis models at the canopy scale in a northern boreal Scots pine forest. *Tellus B: Chemical and Physical Meteorology*, *59*(5), 874–890. https://doi.org/10.1111/j.1600-0889.2007.00305.x

Valentini, R., Matteucci, G., Dolman, A. J., Schulze, E. D., Rebmann, C., Moors, E. J., et al. (2000). Respiration as the main determinant of carbon balance in European forests. *Nature*, *404*(6780), 861–865. https://doi.org/10.1038/35009084

van der Molen, M. K., van Huissteden, J., Parmentier, F.-J., Petrescu, A. M. R., Dolman, A. J., Maximov, T. C., et al. (2007). The growing season greenhouse gas balance of a continental tundra site in the Indigirka lowlands, NE Siberia. *Biogeosciences*, *4*(6), 985–1003. https://doi.org/10.5194/bg-4-985-2007

Vapnik, V. (1995). *The nature of statistical learning theory*. Springer-Verlag.

Vapnik, V., Levin, E., & Cun, Y. L. (1994). Measuring the VC-dimension of a learning machine. *Neural Computation*, *6*(5), 851–876. https://doi.org/10.1162/neco.1994.6.5.851

Veroustraete, F., Patyn, J., & Myneni, R. B. (1996). Estimating net ecosystem exchange of carbon using the normalized difference vegetation index and an ecosystem model. *Remote Sensing of Environment*, *58*(1), 115–130. https://doi.org/10.1016/0034-4257(95)00258-8

Veroustraete, F., Sabbe, H., & Eerens, H. (2002). Estimation of carbon mass fluxes over Europe using the C-Fix model and Euroflux data. *Remote Sensing of Environment*, *83*(3), 376–399. https://doi.org/10.1016/S0034-4257(02)00043-3

Vitale, L., Di Tommasi, P., D'Urso, G., & Magliulo, V. (2016). The response of ecosystem carbon fluxes to LAI and environmental drivers in a maize crop grown in two contrasting seasons. *International Journal of Biometeorology*, *60*(3), 411–420. https://doi.org/10.1007/s00484-015-1038-2

Wang, J., Dong, J., Liu, J., Huang, M., Li, G., Running, S. W., et al. (2014). Comparison of gross primary productivity derived from GIMMS NDVI3g, GIMMS, and MODIS in Southeast Asia. *Remote Sensing*, *6*(3), 2108–2133. https://doi.org/10.3390/rs6032108

Wei, S., Yi, C., Fang, W., & Hendrey, G. (2017). A global study of GPP focusing on light-use efficiency in a random forest regression model. *Ecosphere*, *8*(5), e01724. https://doi.org/10.1002/ecs2.1724

Wohlfahrt, G., Hammerle, A., Haslwanter, A., Bahn, M., Tappeiner, U., & Cernusca, A. (2008). Seasonal and inter-annual variability of the net ecosystem CO_2 exchange of a temperate mountain grassland: Effects of climate and management. *Journal of Geophysical Research: Atmospheres*, *113*(D8), D08110. https://doi.org/10.1029/2007jd009286

Wolanin, A., Camps-Valls, G., Gómez-Chova, L., Mateo-García, G., van der Tol, C., Zhang, Y., & Guanter, L. (2019). Estimating crop primary productivity with Sentinel-2 and Landsat 8 using machine learning methods trained with radiative transfer simulations. *Remote Sensing of Environment*, *225*, 441–457. https://doi.org/10.1016/j.rse.2019.03.002

Wu, C., Munger, J. W., Niu, Z., & Kuang, D. (2010). Comparison of multiple models for estimating gross primary production using MODIS and eddy covariance data in Harvard Forest. *Remote Sensing of Environment*, *114*(12), 2925–2939. https://doi.org/10.1016/j.rse.2010.07.012

Wu, C., Niu, Z., & Gao, S. (2010). Gross primary production estimation from MODIS data with vegetation index and photosynthetically active radiation in maize. *Journal of Geophysical Research*, *115*(D12), D12127. https://doi.org/10.1029/2009JD013023

Wu, H., Zhang, X., Liang, S., Yang, H., & Zhou, G. (2012). Estimation of clear-sky land surface longwave radiation from MODIS data products by merging multiple models. *Journal of Geophysical Research*, *117*(D22), D22107. https://doi.org/10.1029/2012JD017567

Xiao, X. (2004). Modeling gross primary production of temperate deciduous broadleaf forest using satellite images and climate data. *Remote Sensing of Environment*, *91*(2), 256–270. https://doi.org/10.1016/j.rse.2004.03.010

Xiao, X., Boles, S., Liu, J., Zhuang, D., & Liu, M. (2002). Characterization of forest types in Northeastern China, using multi-temporal SPOT-4 VEGETATION sensor data. *Remote Sensing of Environment*, *82*(2–3), 335–348. https://doi.org/10.1016/S0034-4257(02)00051-2

Xiao, X., Hollinger, D., Aber, J., Goltz, M., Davidson, E. A., Zhang, Q., & Moore, B. (2004). Satellite-based modeling of gross primary production in an evergreen needleleaf forest. *Remote Sensing of Environment*, *89*(4), 519–534. https://doi.org/10.1016/j.rse.2003.11.008

Xiao, X., Zhang, Q., Saleska, S., Hutyra, L., De Camargo, P., Wofsy, S., et al. (2005). Satellite-based modeling of gross primary production in a seasonally moist tropical evergreen forest. *Remote Sensing of Environment*, *94*(1), 105–122. https://doi.org/10.1016/j.rse.2004.08.015

Yang, L., Jia, K., Liang, S., Liu, J., & Wang, X. (2016). Comparison of four machine learning methods for generating the GLASS fractional vegetation cover product from MODIS Data. *Remote Sensing*, *8*(8), 682. https://doi.org/10.3390/rs8080682

Yao, Y., Liang, S., Li, X., Chen, J., Liu, S., Jia, K., et al. (2017). Improving global terrestrial evapotranspiration estimation using support vector machine by integrating three process-based algorithms. *Agricultural and Forest Meteorology*, *242*, 55–74. https://doi.org/10.1016/j.agrformet.2017.04.011

Yao, Y., Liang, S., Li, X., Hong, Y., Fisher, J. B., Zhang, N., et al. (2014). Bayesian multimodel estimation of global terrestrial latent heat flux from eddy covariance, meteorological, and satellite observations. *Journal of Geophysical Research: Atmospheres*, *119*(8), 4521–4545. https://doi.org/10.1002/2013JD020864

Yi, C., Anderson, D. E., Turnipseed, A. A., Burns, S. P., Sparks, J. P., Stannard, D. I., & Monson, R. K. (2008). The contribution of advective fluxes to net ecosystem exchange in a high-elevation, subalpine forest. *Ecological Applications*, *18*(6), 1379–1390. https://doi.org/10.1890/06-0908.1

Yi, C., Li, R., Bakwin, P. S., Desai, A., Ricciuto, D. M., Burns, S. P., et al. (2004). A nonparametric method for separating photosynthesis and respiration components in CO_2 flux measurements: Temperature effect on ecosystem light response. *Geophysical Research Letters*, *31*(17). https://doi.org/10.1029/2004GL020490

Yi, C., Monson, R. K., Zhai, Z., Anderson, D. E., Lamb, B., Allwine, G., et al. (2005). Modeling and measuring the nocturnal drainage flow in a high-elevation, subalpine forest with complex terrain. *Journal of Geophysical Research*, *110*(D22), D22303. https://doi.org/10.1029/2005JD006282

Yi, C., Ricciuto, D., Li, R., Wolbeck, J., Xu, X., Nilsson, M., et al. (2010). Climate control of terrestrial carbon exchange across biomes and continents. *Environmental Research Letters*, *5*(3), 034007. https://doi.org/10.1088/1748-9326/5/3/034007

Yuan, W., Cai, W., Xia, J., Chen, J., Liu, S., Dong, W., et al. (2014). Global comparison of light use efficiency models for simulating terrestrial vegetation gross primary production based on the LaThuile database. *Agricultural and Forest Meteorology*, *192–193*, 108–120. https://doi.org/10.1016/j.agrformet.2014.03.007

Yuan, W., Liu, S., Yu, G., Bonnefond, J.-M., Chen, J., Davis, K., et al. (2010). Global estimates of evapotranspiration and gross primary production based on MODIS and global meteorology data. *Remote Sensing of Environment*, *114*(7), 1416–1431. https://doi.org/10.1016/j.rse.2010.01.022

Yuan, W., Liu, S., Zhou, G., Zhou, G., Tieszen, L. L., Baldocchi, D., et al. (2007). Deriving a light use efficiency model from eddy covariance flux data for predicting daily gross primary production across biomes. *Agricultural and Forest Meteorology*, *143*(3–4), 189–207. https://doi.org/10.1016/j.agrformet.2006.12.001

Zhang, L., Zhou, D., Fan, J., & Hu, Z. (2015). Comparison of four light use efficiency models for estimating terrestrial gross primary production. *Ecological Modelling*, *300*, 30–39. https://doi.org/10.1016/j.ecolmodel.2015.01.001

Zhang, Y., Xiao, X., Jin, C., Dong, J., Zhou, S., Wagle, P., et al. (2016). Consistency between sun-induced chlorophyll fluorescence and gross primary production of vegetation in North America. *Remote Sensing of Environment*, *183*, 154–169. https://doi.org/10.1016/j.rse.2016.05.015

Zhang, Y., Xiao, X., Wu, X., Zhou, S., Zhang, G., Qin, Y., & Dong, J. (2017). A global moderate resolution dataset of gross primary production of vegetation for 2000–2016. *Scientific Data*, *4*(1), 170165. https://doi.org/10.1038/sdata.2017.165

Zhao, M., Heinsch, F. A., Nemani, R. R., & Running, S. W. (2005). Improvements of the MODIS terrestrial gross and net primary production global data set. *Remote Sensing of Environment*, *95*(2), 164–176. https://doi.org/10.1016/j.rse.2004.12.011

Zhao, M., Running, S. W., & Nemani, R. R. (2006). Sensitivity of Moderate Resolution Imaging Spectroradiometer (MODIS) terrestrial primary production to the accuracy of meteorological reanalyses. *Journal of Geophysical Research*, *111*(G1), G01002. https://doi.org/10.1029/2004JG000004

Zhou, S., Zhang, Y., Ciais, P., Xiao, X., Luo, Y., Caylor, K. K., et al. (2017). Dominant role of plant physiology in trend and variability of gross primary productivity in North America. *Scientific Reports*, *7*(1), 41366. https://doi.org/10.1038/srep41366

Zielis, S., Etzold, S., Zweifel, R., Eugster, W., Haeni, M., & Buchmann, N. (2014). NEP of a Swiss subalpine forest is significantly driven not only by current but also by previous year's weather. *Biogeosciences*, *11*(6), 1627–1635. https://doi.org/10.5194/bg-11-1627-2014